ERDA/JPL 954355/76-4
Distribution Category UC-63

Mobil Tyco Solar Energy Corporation
16 Hickory Drive
Waltham, Massachusetts 02154

LARGE AREA SILICON SHEET BY EFG

by

A.D. Morrison, K.V. Ravi, C.V. Hari Rao, T. Surek,
D.F. Bliss, L.C. Garone and R.W. Hogencamp

Fourth Quarterly Report - Subcontract No. 954355

Covering Period: October 1, 1976 - December 31, 1976

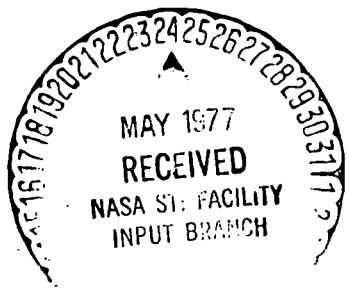

December 15, 1976

"This work was performed for the Jet Propulsion Laboratory, California Institute of Technology, under NASA Contract NAS7-100 for the U.S. Energy Research and Development Administration, Division of Solar Energy.

The JPL Low Cost Silicon Array Project is funded by ERDA and forms part of the ERDA Photovoltaic Conversion Program to initiate a major effort toward the development of low-cost solar arrays."

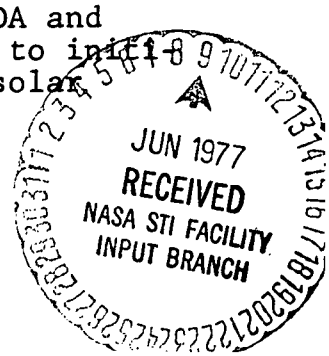

Page Intentionally Left Blank

ABSTRACT

During this reporting period, 5 cm wide ribbons, some with no measurable residual stress, have been grown at speeds up to 5 cm/min. The relationship between residual stress and system vertical temperature gradient was further defined. The problems associated with the purity of the ribbons are being investigated. The influence of light on the recombination characteristics of defects in the ribbons has been investigated.

Page Intentionally Left Blank

Table of Contents

Page Intentionally Left Blank

List of Illustrations

List of Illustrations (continued)

List of Illustrations (continued)

Page Intentionally Left Blank

List of Tables

I. INTRODUCTION

The objectives of this program are to produce at high speeds, thin, wide sheets of silicon of the quality needed to fabricate 10% efficient solar cells. This is part of a total Mobil Tyco Solar Energy Corporation objective to produce silicon ribbon for solar cells at a cost which will allow their wide scale use for generation of electrical power. The edge-defined, film-fed growth process was developed for the commercial production of continuous shaped single crystals of sapphire from the melt and was applied to growth of silicon ribbon for solar cells partly under NSF Grant GI37067X via Harvard University, JPL Contract 953365, and under NSF Grant GI43873. The basic feasibility of the application of EFG to the growth of silicon ribbon has been proven and the theoretical base for extending the technique to the efficient production of sheet silicon has been established.

The two major tasks in this program to produce large area silicon sheet by EFG are: the growth of thin ribbon at high speeds in existing apparatus and the design and construction of a system for the growth of wide ribbons. These two tasks will be combined toward the end of the program to achieve the ultimate program goal. Concurrent with the development of the growth process and ribbon growth apparatus will be material and solar cell characterization programs and theoretical studies of various aspects of EFG silicon sheet growth including melt replenishment, the effect of h_{eff} and aspects of heat flow in the EFG silicon growth system.

Process development and product characterization efforts continued on schedule during the reporting period and are described in the following technical discussion.

Page Intentionally Left Blank

II. TECHNICAL DISCUSSION

A. Ribbon Growth Process

The growth system, JPL No. 1, and its detailed components have been described previously.[1] A preliminary standard operating procedure was submitted to JPL in June, 1976.[2] After eleven growth runs, that procedure is still valid. Various stages in the growth process are illustrated in Figs. 1 - 4. Figure 1 shows the die holder/thermal trimmer cartridge suspended from the seed holder shaft and being lowered into the top of the furnace. Water, gas, and power leads are attached, and the furnace is at temperature. Once equilibrium is attained and the die is filled, a one inch wide EFG silicon seed is dipped and growth is initiated. In Fig. 2, the seed is seen leaving at the top of the picture. A necked region occurs where the operator established end to end thermal balancing and reached growth speed; below, a slowly widening ribbon is seen exiting the cartridge. Once stable ribbon and thermal geometries are achieved (Fig. 3) the operation requires little supervision. In Fig. 4, a full-length ribbon is seen cooling above the growth chamber (the puller stroke is 5 feet). Pieces of ribbon 18-8 are shown in Fig. 5.

B. Results

Eleven ribbon growth runs (Table I) were made during this reporting period on JPL No. 1. These were the first growth efforts on this system. The furnace chamber and main power supply performed very well. First run shortcomings included cartridge to cartridge-power-supply mismatches and cartridge component distortion. This last problem is caused by permeation of SiO into the graphite cartridge parts and subsequent reaction forming silicon carbide. Additional shortcomings were that the hole in the top shield pack was too small for free cartridge access, and that the die extended further into the crucible than expected as a result of thermal expansion of the power studs below and of the cartridge

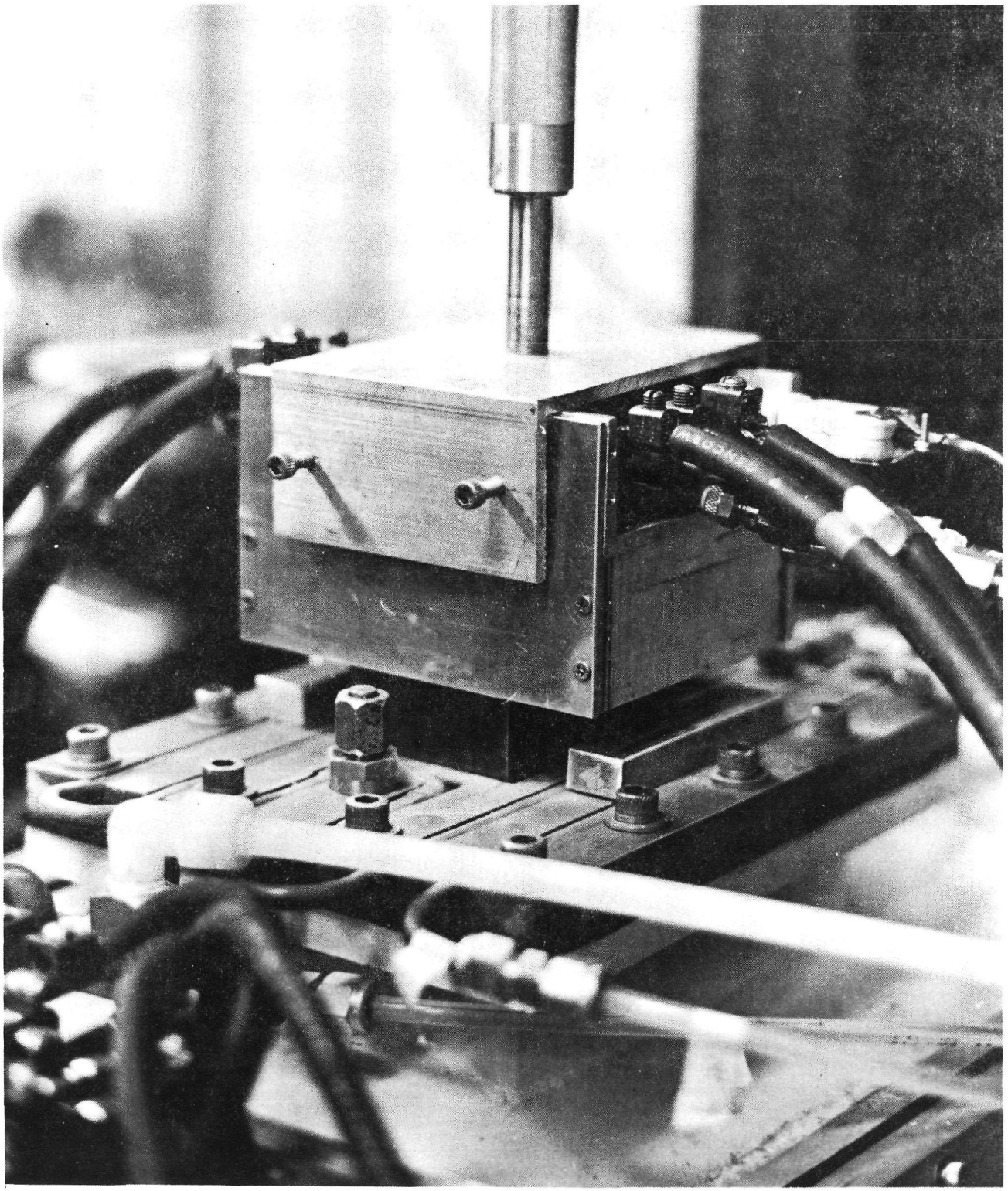

Fig. 1. The die holder/thermal trimmer cartridge suspended from the seed holder shaft. Gas, water, power, and thermocouple lines are connected.

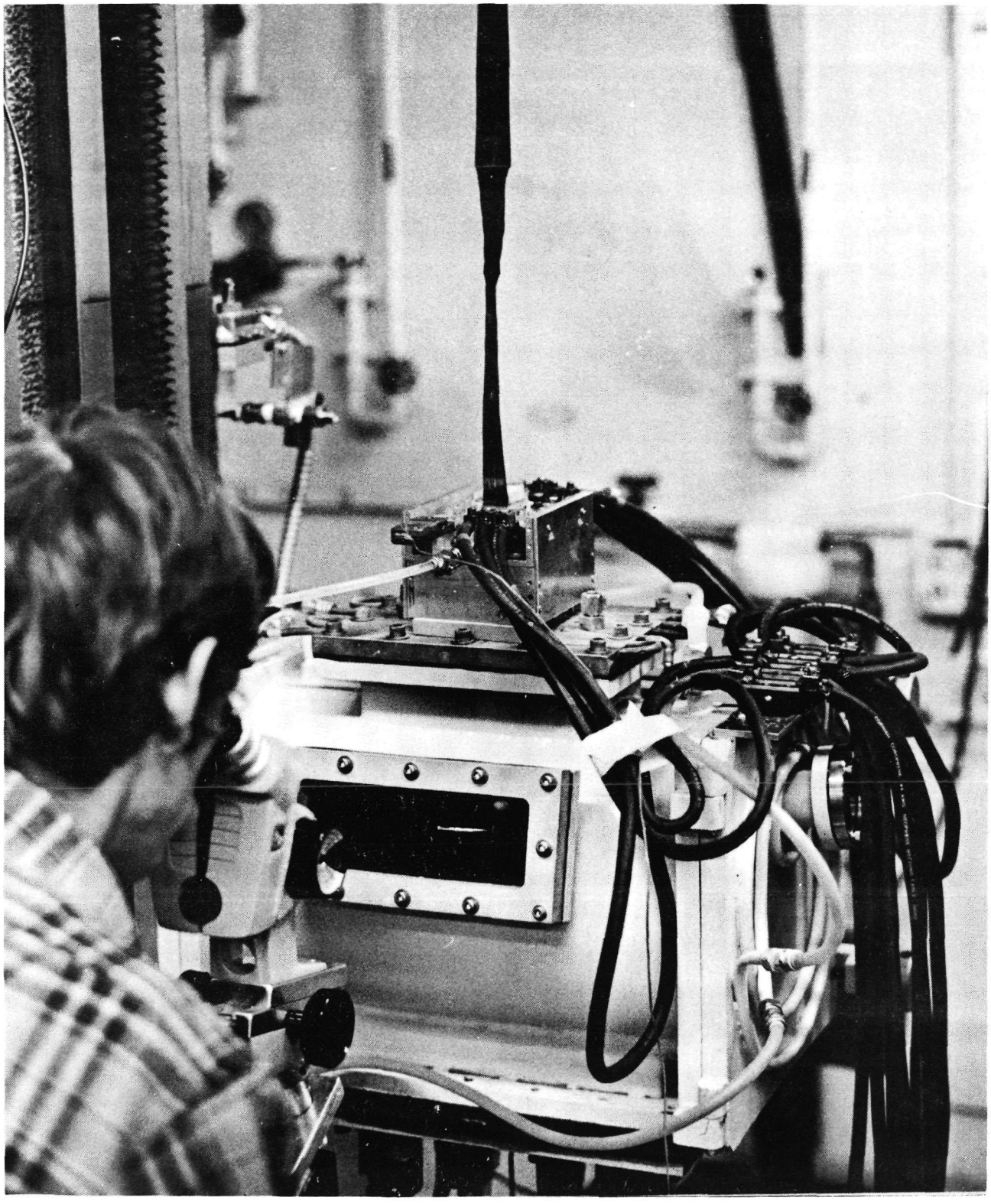

Fig. 2. Growth has begun. The seed is at the top of the picture and a widening ribbon is seen exiting the top of the cartridge.

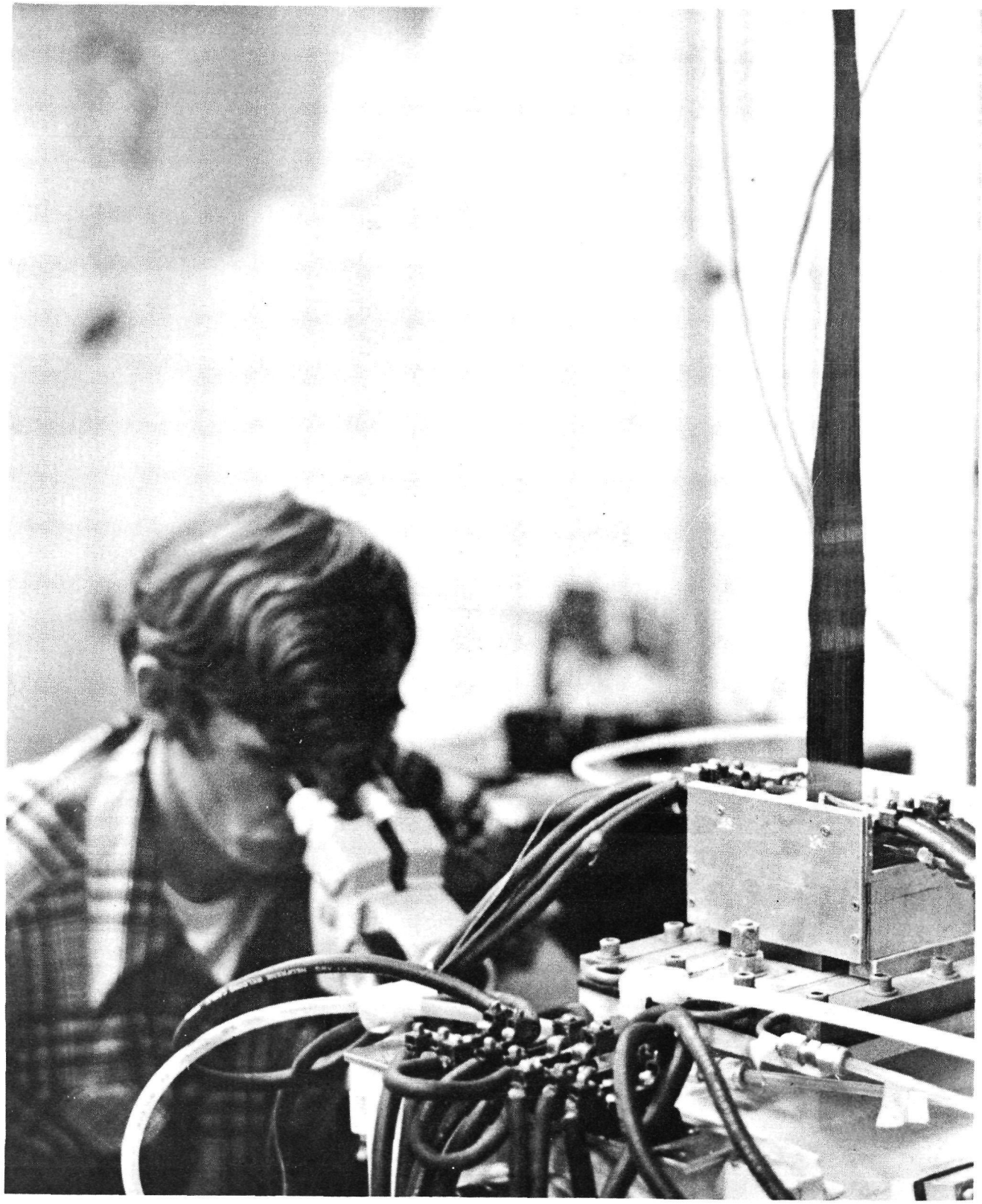

Fig. 3. 5 cm wide ribbon growth.

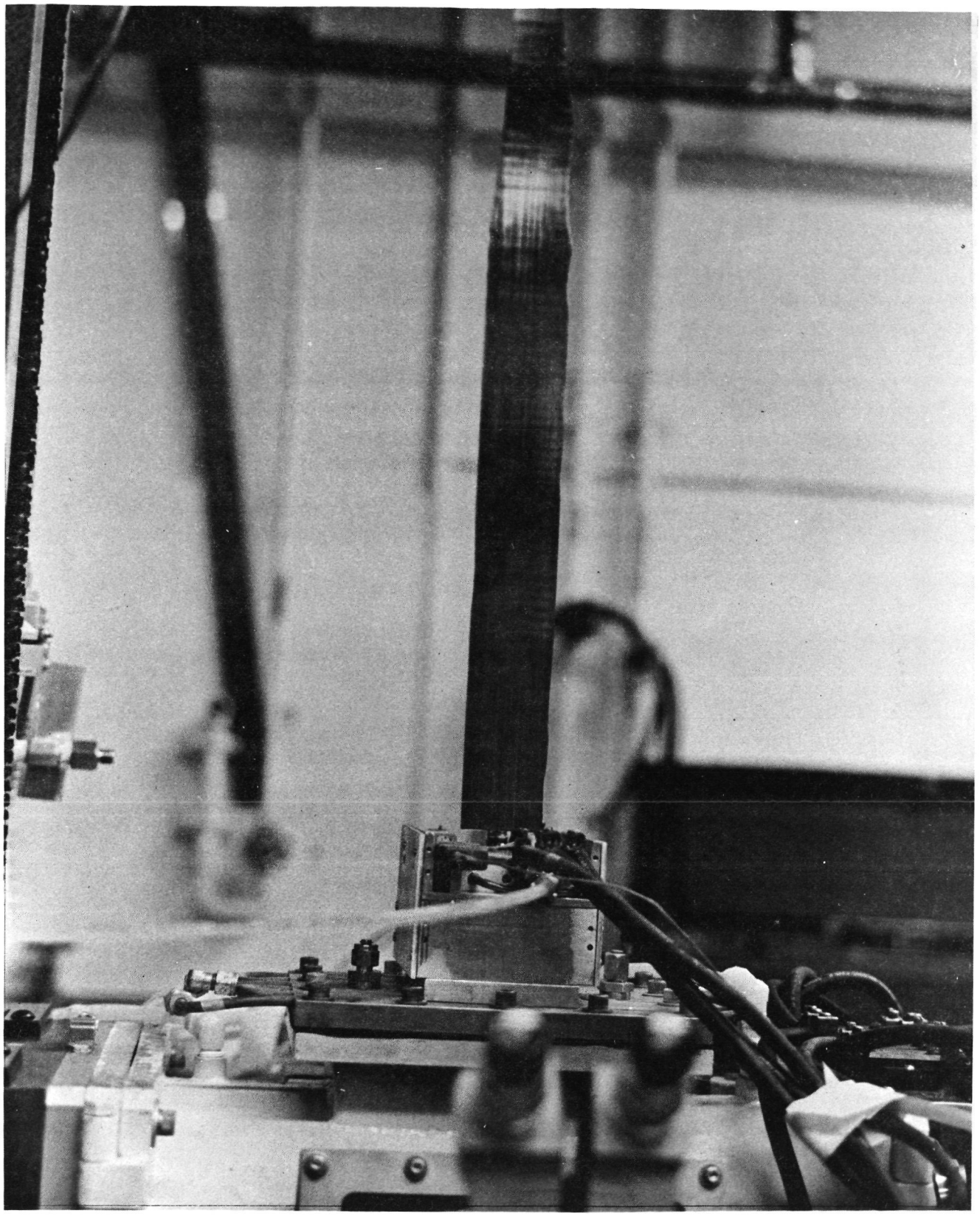

Fig. 4. A 5 cm wide ribbon cools above the growth station.

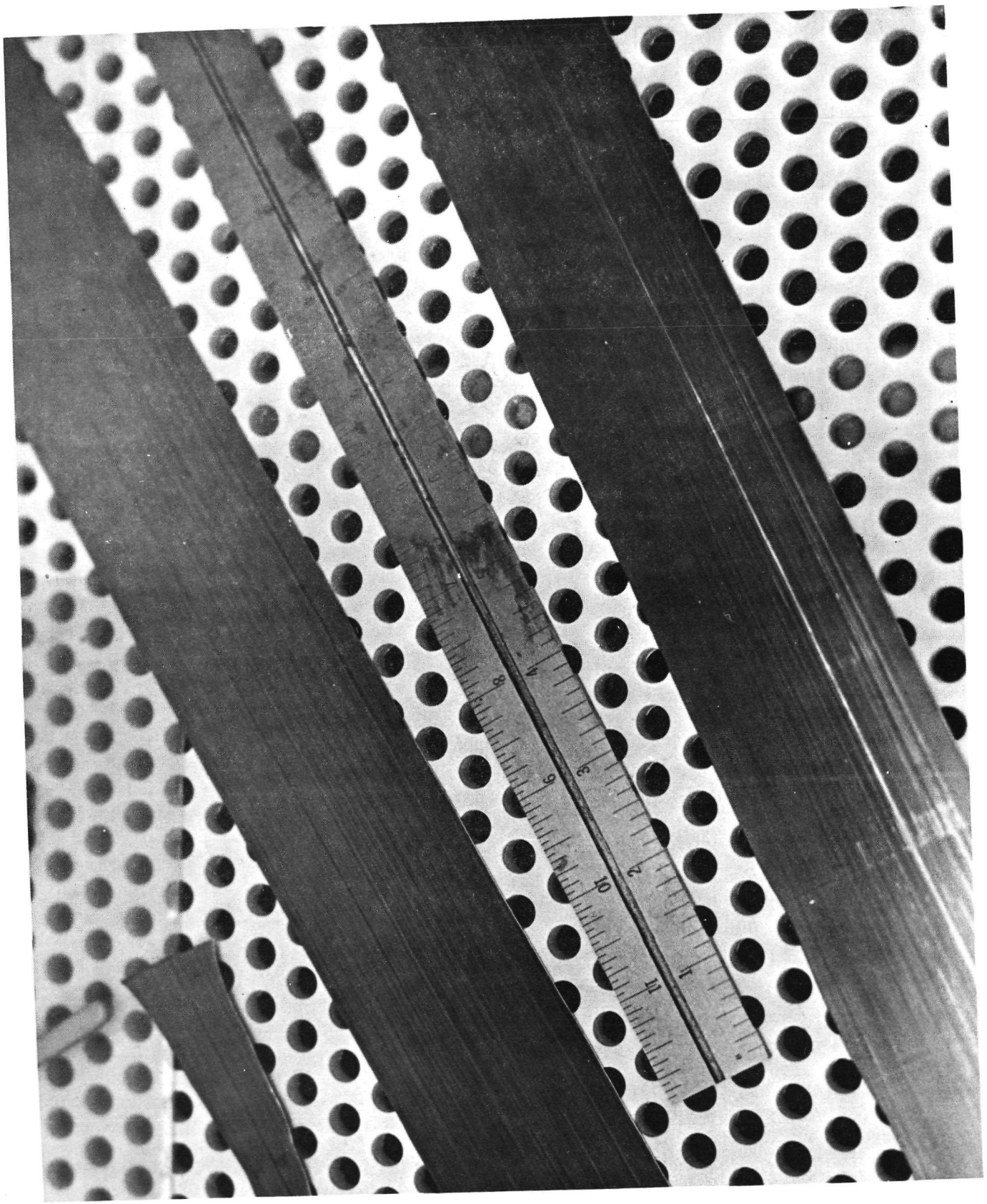

Fig. 5. Pieces of ribbon 18-8 (Table I).

Table I. Growth Run Data - JPL No. 1

RIBBON NO.	DATE	DOPANT	DESIRED Ω·cm	GROWTH RATE cm/min	WIDTH (cm)	LENGTH (cm)	PURPOSE	COMMENTS
18-1-1	09/23/76	Boron	1	3.8	2.5		First growth on JPL No. 1.	Ribbon shattered, after-heater not working.
18-1-2				3.8	1.9 - 2.5	91		He needed for low stress growth.
18-2-1	09/26/76	Boron	1		<.6		To grow 5 cm wide.	Die was too long and stuck into quartz crucible below.
18-2-2				3.2	Up to 3.8			
18-3-1	10/05/76	Boron	1		<2.5		To grow 5 cm wide.	Use of He drains heat from afterheater. Thickness 3 - 8 mils.
18-3-2				3.2	2.5			
18-3-3				3.8	4.6			No apparent frozen-in stress.
18-4	10/18/76	Boron	1				To grow 5 cm wide, 5 cm/min.	SCR controller failed.
18-4-1	10/21/76	Boron	1	4.3	<2.5	7.6		
18-4-2				4.3	3.4	101		All Al_2O_3 system components removed. On the occasion of every freeze, an oxide-SiC coating was deposited on the ribbon opposite the cooling gas ports. Die was too long, again.
18-4-3				4.3	4	114		
18-4-4				4.3	4.45	127		
18-4-5				5.1	3.5	53		
18-4-6				4.3	4	101		
18-5-1	10/29/76	Boron	1	3.8	1.9 - 3.8	89	To grow 5 cm wide, 5 cm/min.	End heaters not controlling. 13 - 16 mils thickness.
18-5-2				3.8	2.1 - 2.8	96		
18-5-3				3.8	1.9 - 2.5	81		
18-6	11/18/76	Boron	10	5	<2.5	8.8	To characterize 10 $\Omega \cdot cm^{-1}$ doped ribbon.	Die splayed, became misaligned terminating growth. Melt overheated.
18-7	11/24/76	Boron	10	2.5 - 3.1	3.75	~90	To profile temperatures, to improve on 18-6.	Melt overheated. SiO vacuum cleaner plugged up early in run.
18-8-1	12/03/76	Boron	10	2	2.5 - 5	79	To grow 5 cm wide at 5 cm/min.	½ to JPL, ½ to seeds.
-2				2	2.5 - 5	132		Stock.
-3				3.8	<5			
-4				2 - 5.5	2.5 - 5	71		For evaluation.
-5				2 - 5	2.5 - 5	89		Solar cell evaluation. 6.3% efficient 1" x 4" cell obtained.
18-9	12/07/76					0		Cartridge shorted.
18-10-1	12/10/76	Boron	1	2.5	3.8	58	Same as 18-8.	Cartridge shorted but was repaired.
-2				2.5	4.4	46		
-3				2.5	4.9	48		
-4				2.5	5	94		
-5				2.5	5	46		
-6				2.5	5	64		
-7				2.5	5	56		
18-11-1	12/14/76	Boron	1	4.3	<2.5	76		Wacker crackle.
-2				4.3	2.5	51		
-3				4.3	3.1	41		
-4				4.3	5	79		
-5				4.3	5	132		
-6				4.3	5	91		Very high gas flows.

above. Despite the fact that the capillary at the bottom of the die was partially plugged by silica from the crucible, approximately 91 cm of ~3.25 cm wide ribbon was grown on the first growth attempt. Power supplies for the cartridge heaters were modified and a second run was made. Ribbon up to 3.25 cm wide was grown at speeds up to 3.25 cm per minute. Both of these were "learning runs" developing operator familiarity with the system, and trouble shooting. They were designated growth attempts 18-1 and 18-2. To keep the die from sticking into the bottom of the silica crucible, the height of the cartridge was increased for growth Run No. 18-3. Ribbon up to 4.6 cm in width was grown at speeds of about 3.25 cm per minute. The ribbon split longitudinally because of mishandling rather than as a result of frozen-in stress.

Run 18-4 was attempted on two separate occasions. The first effort failed due to electronics malfunctions. The entire main power supply SCR controller was replaced by the manufacturer and the ribbon growth run was finally made. More than five meters of ribbon up to 4.45 cm wide was grown at speeds up to 5 cm per minute. Nearly all was stress-free (Table II). (Samples with stress ripples or buckles were measured to have a residual stress of about 11,000 psi). The die in this run was again too long, but growth was achieved despite the fact that the bottom of the die was jammed into the soft silica crucible. Films containing oxides and SiC occurred on the ribbon. Ribbon growth effort 18-5 yielded 2.7 meters of material up to 3.8 cm wide grown at rates up to 3.8 cm per minute. This material was grown from an alumina free but not totally baked out system. Difficulty achieving full-width growth was common to the above runs. Run Nos. 18-6 and 18-7 were efforts to achieve 5 cm ribbon growth width, to grow for characterization from 10 $\Omega \cdot$cm melts, and to begin to profile the temperatures in the cartridge. Neither ribbon growth run was successful. The first failed when the die splayed open beneath the cartridge floor and both heat and liquid flows became unpredictable and uncontrollable. No useful length of ribbon was grown. Although splaying of the die halves has been common in other growth systems, this is the only time it has occurred since JPL No. 1 has been in service. A vacuum system intended to reduce the SiO vapors above the melt was put into operation after a melt was achieved. Between $\frac{1}{4}$ and $\frac{1}{2}$ of the total purge gas flow (~30 scfh) was drawn from the plenum above the melt. No substantial SiO precipitates were found in the piping to the pump and no apparent reduction of the usual SiO deposits on the cartridge and heat shields was observed. The vertical thermal gradient above the die was measured, shown in Fig. 6. The second growth effort,

Table II. Ribbon Stress

RIBBON NO.	GROWTH RATE (cm/min)	STRESS (psi)	COMMENTS
18-3-3	3.8	0*	Broke during handling.
18-4-2	4.3	0*	No measurable gap by scribe and split test.
18-4-?	4.3	11,270	Rippled ribbon, scribed square in both directions.
18-4-5	5.1	0*	Despite deep scribing, would not split lengthwise.
18-5-3	3.8	4,600	Afterheater 1200°C, ambient was He.

*<Limits of measurement

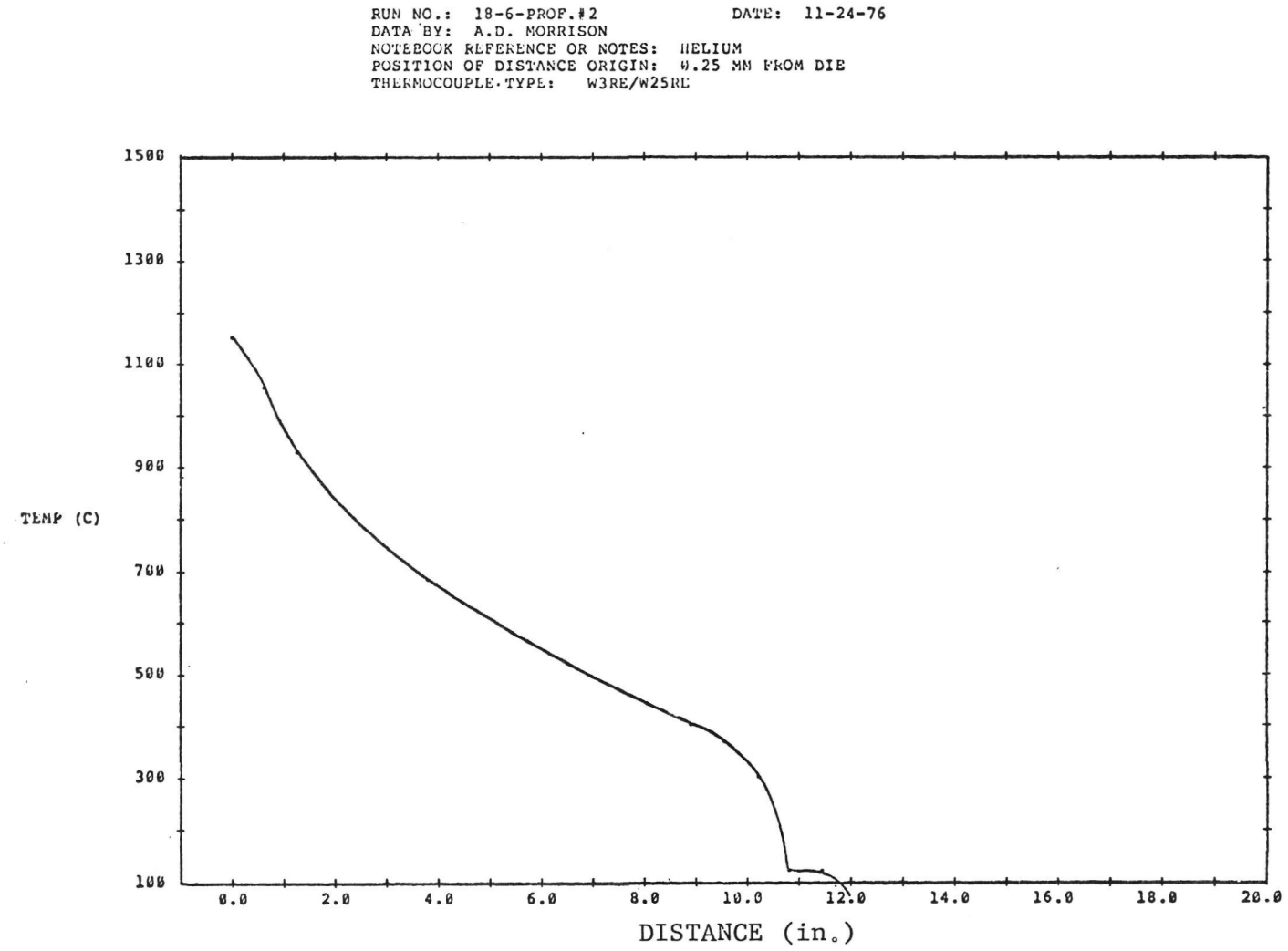

Fig. 6. Growth system temperature profile (Run No. 18-6).

Run No. 18-7, also did not achieve its purpose. No ribbon wider than ~3.75 cm was grown. This was apparently because the melting point isotherm was 'bumpy'; e.g., cold at the ends of the die, and hottest at points ~7 mm from each end of the die. It is not possible to spread a narrow ribbon to full width under these circumstances. It was observed on shut down that the crucible walls had slumped appreciably and that the whole crucible was greatly devitrified, indicating that the melt was greatly overheated; a condition which would explain the poor growth results. Large deposits of SiO were observed to form on the heat shields throughout the run. It clogged the moly tubes from the vacuum system.

Growth Run 18-8 yielded >3 meters of ribbon, the greater part of which was 5 cm wide. The charge was 10 Ω·cm doped Wacker crackle silicon. Although the die top was the same as in all previous runs, the bottom was one-piece, slotted along the edges for capillaries. The ribbon grew easily; spreading and edge stability were controlled by the end heaters alone. Growth rates up to 5.5 cm/min were achieved. The vertical thermal profile of the system is shown in Fig. 7. Characterization of the electronic properties of this material is reported elsewhere in this report. Because of electrical shorts in the cartridge, Run 18-9 was prematurely terminated; no material was grown. In Run 18-10, >3.3 meters of ribbon up to 5 cm wide was grown from 1 Ω·cm doped Wacker crackle material without difficulty. Growth rates were ~2.5 cm/min. Run 18-11 was similar to the previous run except that pull rates were ~4.3 cm/min. Ribbon No. 18-11-6 was grown with a very high cartridge gas flow. The only obvious effect during growth was that it was difficult to maintain edge stability.

C. Residual Stress Versus Vertical Temperature Profile

1. Theory

The previous annual report[1] has described in detail the theory of thermal stresses in ribbon crystals grown by the EFG technique. A new design strategy, involving a cooling/afterheating block configuration, which minimizes the residual stress in the ribbon and, at the same time, allows the desired fast growth rates was also described. As previously reported, initial in-house experiments, using a cartridge design developed on an MTSEC in-house program,[3] have resulted in essentially stress-free ribbons grown at rates in excess of 5 cm/min and with widths up to 5 cm. In this section, we report on some theoretical calculations which indicate the extent to which the various design variables in the cooling/afterheating block influence the thermal profile

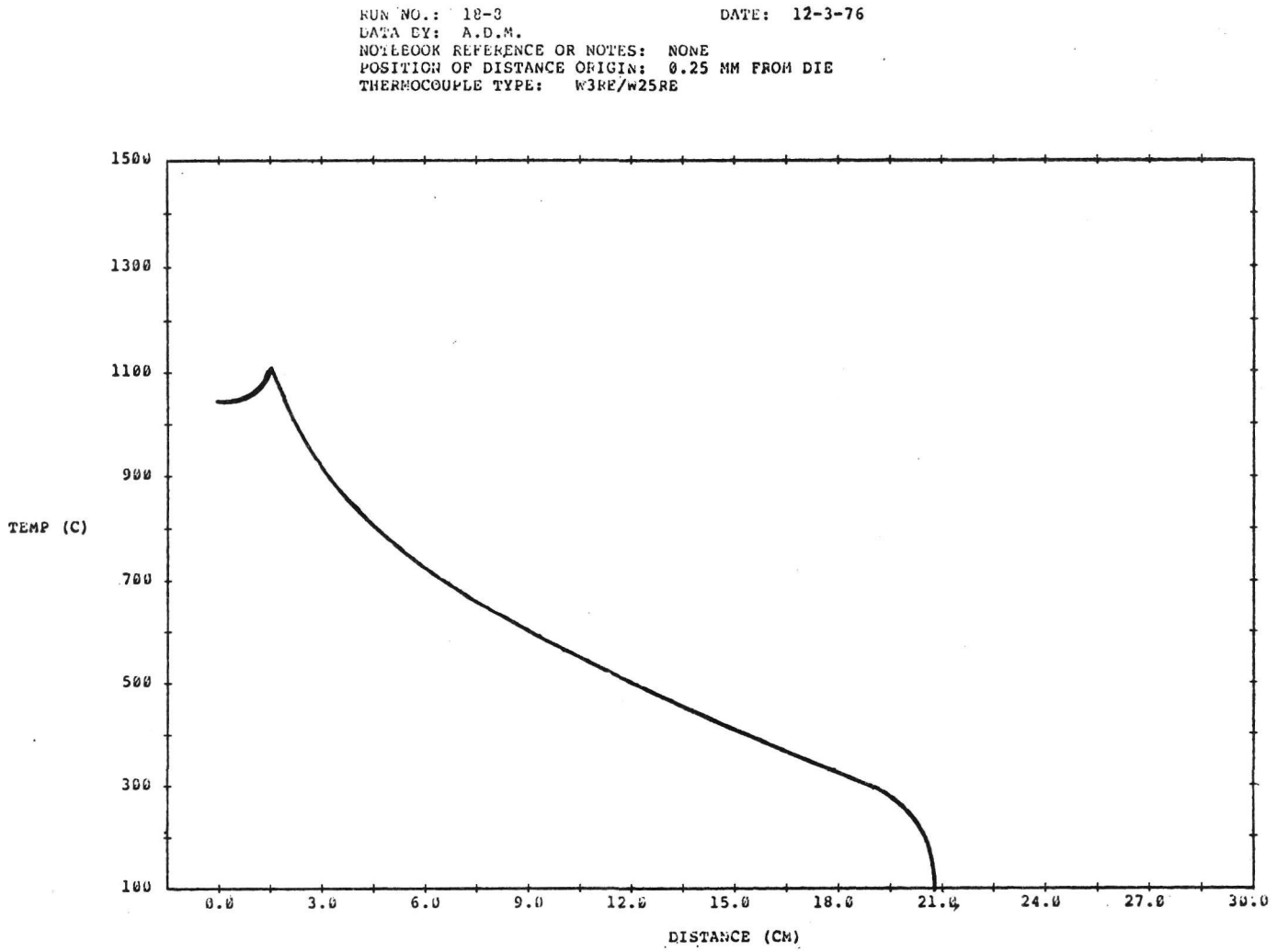

Fig. 7. Growth system temperature profile (Run No. 18-8).

in the ribbon, and hence the growth rates and residual stresses which are to be expected. In the next section, we present the results of experiments on fast, stress-free ribbon growth.

A schematic of the cooling/afterheating block configuration is shown in Fig. 8(a). The thermal environment of the ribbon consists of five distinct regions, as indicated in the figure; this is representative of the experimental arrangement described later in this section. The temperatures in the shielding and radiation regions (T_S and T_R, respectively) correspond to the effective temperatures in the regions beneath the growth interface and in the low angle viewing region beneath the cold block. The cooling/afterheating block is at a distance Y_B above the growth interface, while the distance from the ribbon is X_B (the block spacing is $2X_B + t$, where t is the ribbon thickness; t = 10 mils was used in the calculations described below). The variables Y_C and Y_I denote, respectively, the heights of the cooling and insulation zones. The actively powered afterheater region is designed to give a linear gradient G_H along the block; the power is adjusted to give a maximum temperature T_{MAX}, as shown in Fig. 8(a). The cooling region is assumed to be at a constant temperature T_C; the temperature of the insulation region is assumed to be $T_I = \frac{1}{2}(T_C + T_{MAX})$.

The details of the computer model used to calculate the steady-state temperature profile in the ribbon were described in the previous report.[1] Briefly, the model considers conductive and convective heat transport in the ribbon, and radiative and convective cooling at the ribbon surface. Heat flow in the ribbon is assumed to be one-dimensional, i.e., the vertical temperature profile is calculated. The radiative heat flux is determined from the temperatures, emissivities and angle factors of the surfaces which comprise the thermal environment of the ribbon. The convective cooling (or heating) at the ribbon surface involves a heat exchange through the gas ambient between the ribbon and the block at each point; a value of Nu = 6 has been assumed for the Nusselt number for convective heat transfer.

The vertical temperature profile which is expected to lead to the desired fast growth rates and minimal residual stresses in the ribbon is shown schematically by the broken line in Fig. 8(b). As described previously,[1] the vertical temperature profile, ideally, should consist of three zones. The first zone (from the melting point to ~1200°C) should consist of an initially large temperature gradient and a very rapid decrease of the gradient away from the growth interface. The

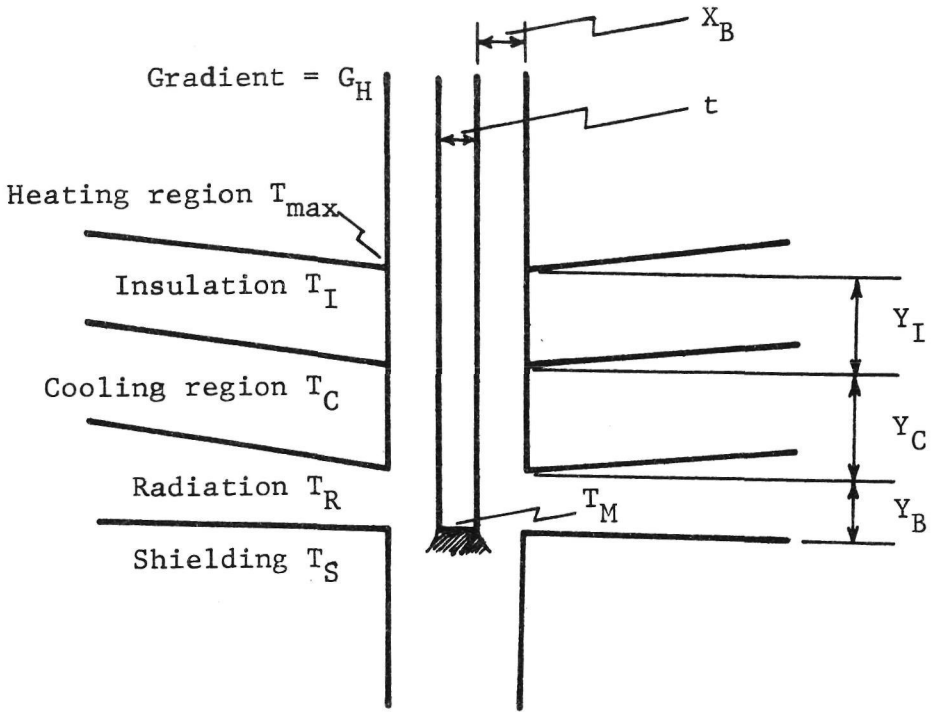

(a)

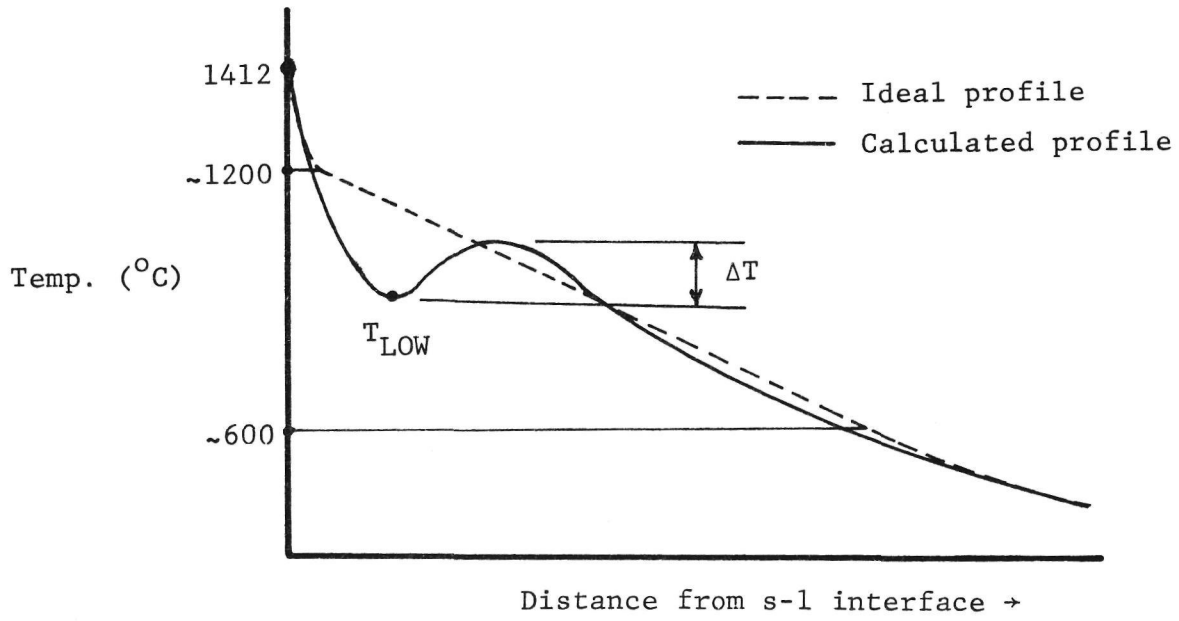

(b)

Fig. 8. (a) Schematic of cooling/afterheating block configuration showing variables used in analysis. (b) Schematics of ideal and actual (calculated) vertical temperature profiles in ribbon.

second zone should be a region of constant temperature gradient from ~1200°C to ~600°C, while the third zone should consist of a further decrease in gradient that is needed to reach zero gradient at room temperature.

The feasibility of the above concept for the vertical temperature profile in the ribbon was studied extensively for the cooling/afterheating block configuration in Fig. 8(a). The computer calculations were used on a MTSEC in-house program[3] in the design and development of the 2 in. cartridge chamber with built-in cooling/afterheating blocks. This cartridge was transferred to the current JPL program, and has been used in the 2 in. wide ribbon growth runs during this quarterly period, as described elsewhere in this report. The results of the calculations are summarized in Tables III and IV for argon and helium gas ambients, respectively. Case a in Table III represents the "standard" values, for the case of argon, with respect to which variations in the various parameters were considered (case A in Table IV is the standard for a helium ambient). Because of the considerable cooling in the initial portion of the ribbon (which is a result of the particular choices T_S = 1200°C, T_R = 700°C, Y_B = 40 mils, T_C = 200°C and Y_C = 50 mils), the resulting profile typically consists of a minimum in temperature (T_{LOW}) followed by a maximum in the afterheating region (see solid line in Fig. 8(b)). The sharp positive and negative curvatures in the temperature profile are likely to be undesirable both for obtaining a low density of plastic strain induced imperfections and for a low value of the residual elastic stress in the ribbon. Values of T_{LOW}, the amount of reheating in the ribbon (ΔT), and the second derivative in the profile at T_{LOW} are given in the tables. Within the linear gradient zone of the afterheater, the temperature profile in the ribbon soon attains that in the afterheater block.

The quantity V_{max} in the tables represents the maximum growth rate which may be expected for each given set of conditions. These values were determined from stationary (i.e., zero growth rate) temperature profiles; the effect of convective heat transport[1] in the growing ribbon leads to actual (calculated) maximum rates which are about 10 to 20% lower than the V_{max} values given in the table. It is readily seen in the tables that an increase in ribbon growth rate may be achieved either by increasing the value of Y_C, or by decreasing the values of any one or more of the parameters T_M, T_R, T_S, T_C, X_B and Y_B.

The sensitivity of the growth velocity to variations in each of the

Table III. Cooling/Afterheating Block Calculations for Argon Ambient

	Distance from ribbon	Shielding	Radiation region		Cooling region		Insulation region		Heating region		Results			
	X_B mils	T_S °C	T_R °C	Y_B mils	T_C °C	Y_C mils	T_I °C	Y_I mils	G_H °C/cm	T_M °C	T_{Low} °C	ΔT (approx.) °C	d^2T/dx^2 at T_{Low}	V_{max} in./min
a	30	1200	700	40	200	50	700	50	35.4	1200	1109	54	4088	2.82
b	"	"	"	"	"	"	675	"	"	1150	1087	40	3856	2.90
c	"	"	"	"	"	"	650	"	"	1100	1063	10	3408	3.01
d	"	"	"	"	"	100	700	"	"	1200	1009	120	5552	3.26
e	"	"	"	"	"	"	675	"	"	1150	993	97	4176	3.33
f	"	"	"	"	"	"	650	"	"	1100	971	62	2816	3.41
g	"	"	"	"	"	150	700	"	"	1200	917	162	4296	3.59
h	"	"	900	"	"	50	"	"	"	"	1111	52	4096	2.75
i	"	"	500	"	"	"	"	"	"	"	1107	55	4224	2.86
j	"	1300	700	"	"	"	"	"	"	"	1111	50	4256	2.76
k	"	1100	"	"	"	"	"	"	"	"	1109	60	4260	2.85
l	"	1200	"	"	400	"	800	"	"	"	1128	45	3488	2.64
m	"	"	"	"	0	"	600	"	"	"	1094	75	4672	2.96
n	15	"	"	"	200	"	700	"	"	"	1055	110	5664	3.47
o	45	"	"	"	"	"	"	"	"	"	1131	40	3088	2.54
p	60	"	"	"	"	"	"	"	"	"	1140	35	2624	2.37
q	75	"	"	"	"	"	"	"	"	"	1143	30	712	2.27
r	30	"	"	20	"	"	"	"	"	"	1139	21	4264	2.96
s	"	"	"	60	"	"	"	"	"	"	1083	90	4016	2.72

Table IV. Cooling/Afterheating Blcok Calculations for Helium Ambient

	Distance from ribbon	Shielding	Radiation region		Cooling region		Insulation region		Heating region		Results			
	X_B mils	T_S °C	T_R °C	Y_B mils	T_C °C	Y_C mils	T_I °C	Y_I mils	G_H °C/cm	T_M °C	T_{Low} °C	ΔT (approx.) °C	d^2T/dx^2 at T_{Low}	V_{max} in./min
A	30	1200	700	40	200	50	700	50	35.4	1200	865	308	23200	5.81
C	"	"	"	"	"	"	650	"	"	1100	838	239	21400	6.00
L	"	"	"	"	400	"	800	"	"	1200	923	254	20800	5.14
M	"	"	"	"	0	"	600	"	"	"	814	363	25100	6.42
N	15	"	"	"	200	"	700	"	"	"	747	433	31600	7.61
O	45	"	"	"	"	"	"	"	"	"	931	246	18900	4.92
P	60	"	"	"	"	"	"	"	"	"	975	189	6600	4.36
Q	75	"	"	"	"	"	"	"	"	"	1005	38	6130	3.96
R	30	"	"	20	"	"	"	"	"	"	913	260	26900	7.17
S	"	"	"	60	"	"	"	"	"	"	832	340	21100	4.98

cooling/afterheating block parameters is examined further in Table V. Assuming that the growth velocity varies linearly with all the variables, we show in this table the change which would be required in any of the parameters in order to obtain a 10% increase in growth velocity. It is seen that the growth velocity is relatively independent of the temperatures in the shielding and radiation region, but that it is quite sensitive to the temperature and extent of the cooling zone, and to the position of the block with respect to the growth interface and the ribbon. The height, Y_B, of the block above the growth interface also has a large influence on the temperature profile. For example, decreasing Y_B from 40 to 20 mils (cases a and r in Table III) not only increases the growth velocity, but it also decreases the extent of the overshoot (i.e., ΔT) in the temperature profile. The sensitivities of the growth velocity and of the profile to the block parameters depend, of course, on the particular set of values of the parameters. For higher values of the temperatures T_S, T_R and T_C, the geometrical variables X_B, Y_B and Y_C are expected to have a greater influence on the ribbon profile and on the growth velocity.

The conclusion we reached from these calculations is that a relatively simple block configuration (in terms of the temperatures and distances involved) should enable us to obtain the desired temperature profile in the ribbon for fast, stress-free growth. From the V_{max} values in the tables, we see that the program goal of 3 in./min should be attainable using an argon ambient, or a mixed argon-helium ambient. As indicated, we have assumed in the calculations that the Nusselt number for the convective heat exchange between the ribbon and the block is equal to 6. In the limiting case where Nu = 1, the effective cooling of the ribbon would be less; for the conditions in case a in Table III, we obtain V_{max} = 2.26 in./min (with $T_{LOW} \simeq 1156^{\circ}C$ and $\Delta T \simeq 10^{\circ}C$).

2. Experimental Results

Experimental work to evaluate the effects of the vertical temperature profile on growth rate and residual stress in ribbons has been carried out on both growth stations (JPL No. 1 and JPL No. 2) during this quarterly period. The runs on JPL No. 1 used the cartridge design with the built-in cooling/afterheating regions, as described elsewhere in this report. In many of these runs, the ribbons that were grown were full-width (i.e., 5 cm wide), and growth rates in excess of 5 cm/min were attained (see Table I). The residual stress in the ribbons was low enough (see Table II) that the ribbons could be readily cut into

Table V. Variations in Cooling/Afterheating Block Parameters for 10% Increase in Growth Velocity*

Variable	Gas Ambient: Argon	Gas Ambient: Helium
T_M	decrease by 148°C	306°C
Y_C	increase by 36 mils	-
T_R	decrease by 1025°C	-
T_S	decrease by 627°C	-
T_C	decrease by 353°C	182°C
X_B	decrease by 9 mils	6.5 mils
Y_B	decrease by 47 mils	10.6 mils

*Standard conditions are cases a and A in Tables III and IV, respectively; the growth velocity is assumed to vary linearly with all the variables.

solar cell blanks. Typical temperature profiles measured in the cartridge setup were shown in a preceding section (e.g., Fig. 7).

In the experiments on JPL No. 2, a specially designed graphite cold block/afterheater combination was used (see Fig. 9 and Figs. 27 - 38). The graphite cold block is a modified version of that used in previous fast growth experiments on this program (e.g., Fig. 2 of Ref. 4). In those experiments, growth rates of >5 cm/min were reached, but the ribbons were excessively stressed. In the setup of Fig. 9, the extent of the cooling region (Y_C in the notation of the previous section) could be readily varied by changing the cooling block; in the experiments reported below, we used a block with Y_C = 0.635 cm and a spacing (i.e., $2X_B$ + t) of 0.457 cm. The entire assembly in Fig. 9 can be translated vertically to attain a desired height (i.e., Y_B) above the growth interface. The temperature profile in the afterheater region is controlled by the location and size of the heater rods, by the power dissipated in the rods, and by the dimensions of the thermal gradient plate. In two of the current experiments, a 0.33 cm diameter graphite heating rod was used at location No. 1 in Fig. 9; in a third experiment, an additional heating rod (0.224 cm diameter) was used at location No. 2. The dimensions of the graphite thermal gradient plates were 20.1 cm x 4.19 cm x 0.127 cm; the spacing of the plates was 0.152 cm. Two thermocouples were inserted in the graphite cold block to monitor the block temperature; these were located ~0.08 cm and ~0.16 cm, respectively, from the cooling surface of the block. The vertical temperature profile in the afterheater region was determined by traversing a thermocouple through the afterheater.

Three growth runs (Nos. 14-203, 14-204 and 14-205; see Table VI) were made during this period using this cold block/afterheater assembly. In Run No. 14-203, six short ribbons, ~1.5 cm wide, were grown at speeds from ~3.8 cm/min to ~6.8 cm/min. The growth was purposely interrupted when efforts to increase the ribbon width failed, and a new, full-width seeding was attempted. All of the ribbons had considerable residual stress as evidenced by the splitting of the ribbons after scribing. The stresses were much lower, however, than those obtained using the graphite cooling blocks alone in some past experiments on this machine.[4]

Figure 10 shows examples of the vertical profile in the cooling/afterheater unit in Run No. 14-203. The distance is measured from the lower tip of the graphite cooling blocks; the distance of the cold block from the die, and the various heater settings are noted in the figure.

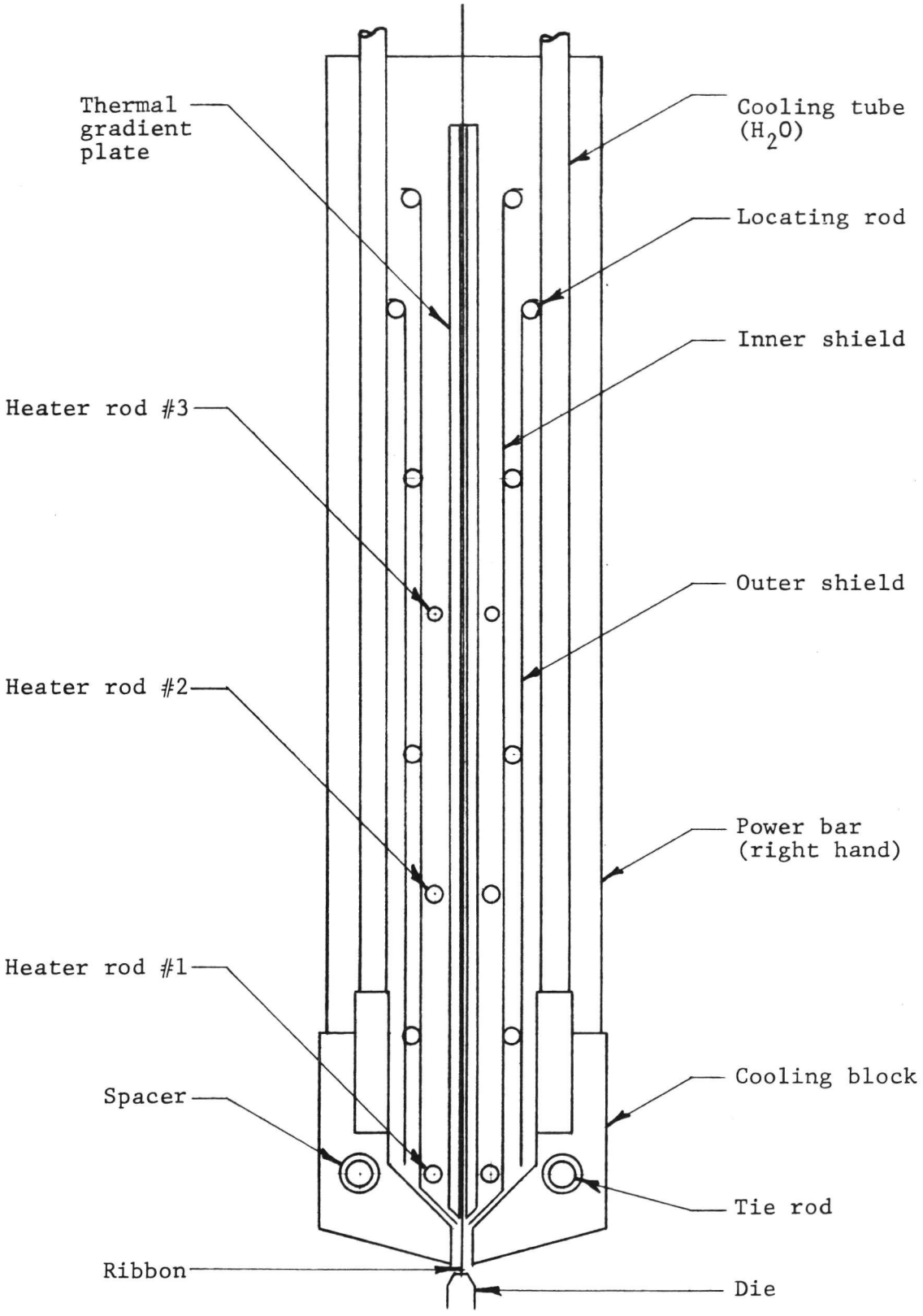

Fig. 9. Heat sink/afterheater assembly for JPL No. 2.

Table VI. Growth Run Data - JPL No. 2

RIBBON NO.	DATE	DOPANT	DESIRED Ω·cm	GROWTH RATE cm/min.	WIDTH (cm)	LENGTH (cm)	PURPOSE	COMMENTS
14-203	11/12	B	1	3.8 - 6.8	<2.5	152	to relate growth rate, stress, and vertical gradients.	guidance problems cause ripples in ribbon; residual stress large.
14-204	11/19	none	-	2.5 - 6.75	<2.5	~75	same as 203.	buckling every 2 - 2.25 cm; residual stress large.
14-205	11/24	B	1	5 - 6.75	2.5	217	same as 203.	buckling every 2 - 3 cm; no residual stress in ribbons.

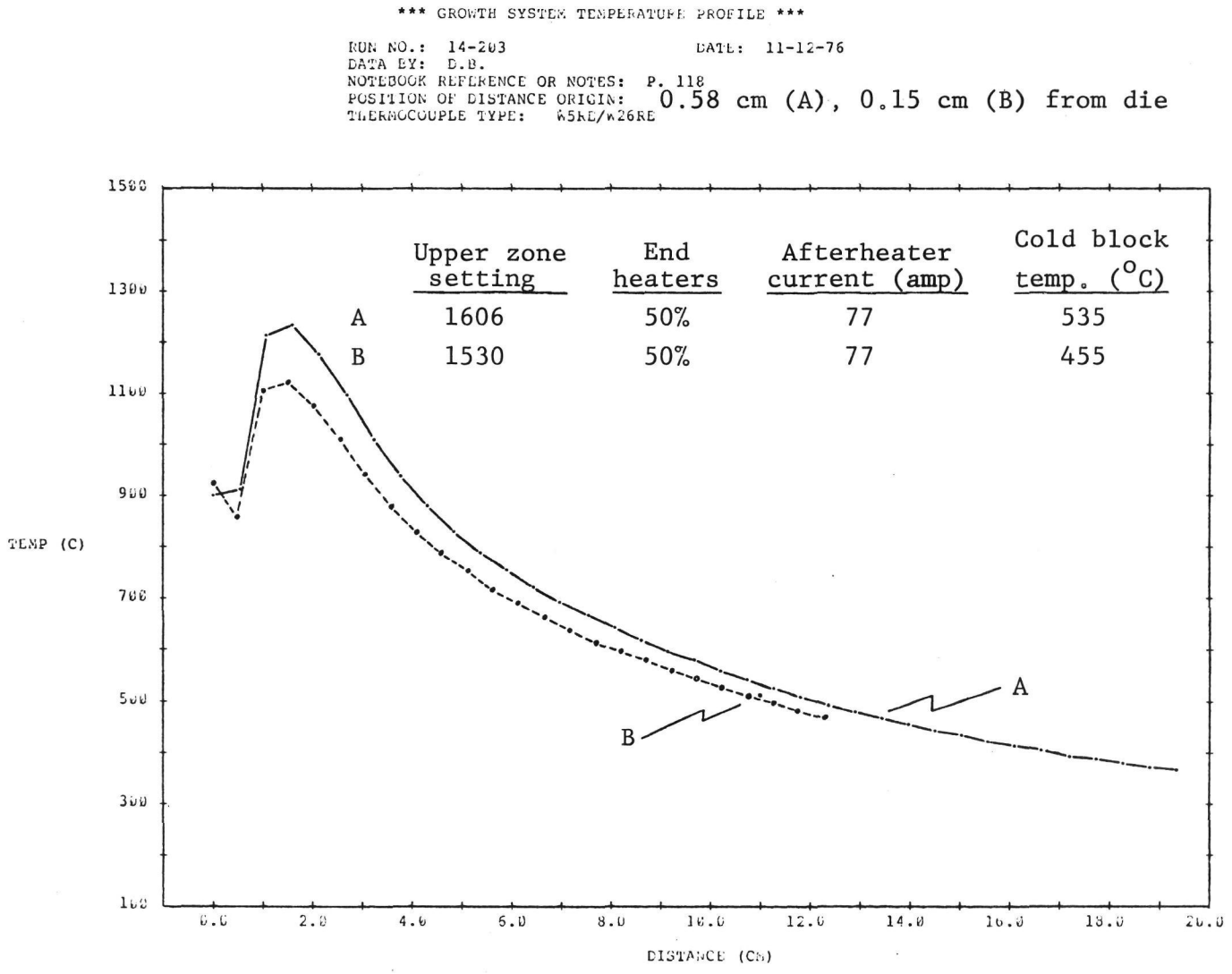

Fig. 10. Vertical temperature profiles measured in Run No. 14-203.

Although the power to the afterheater is the same for both curves, the cold-block temperature and the entire vertical profile are seen to be affected by the heat fluxes from the die, and the face and end heaters. The early portions of the curves, up to the maximum, do not represent the true temperature profile; in this region, the thermocouple is exposed to various hot (e.g., die, face heater) and cold radiative surfaces. The cold-block temperatures recorded by the thermocouple in the block are given in the figure; the actual profile in the ribbon needs to be calculated from theory, as in the preceding section, for these measured environmental conditions.

The probable reason for the residual stress in the ribbons from Run No. 14-203 is apparent from Fig. 10; the profile in the afterheater (hence in the ribbon) was not linear, as required, in the region from ~1200°C to ~600°C. The non-linearity of the afterheater profile was to be expected, as the graphite thermal gradient plate has a large radiating surface to conducting cross-section ratio. Also, no allowance has been made in the design for the variation of thermal conductivity of the graphite with temperature.

Run No. 14-204 used the same cold block/afterheater setup as in Run No. 14-203 but with a radiused die; it was felt that the latter would permit spreading (hence full-width) growth which was not possible with the flat die used in 14-203. Indeed, nearly full-width growth at rates between 5 cm/min and 7.5 cm/min was achieved; the ribbons were excessively buckled and had a fairly large residual stress, as determined by scribing and splitting. The buckling was partially caused by misalignment between the puller and the block assembly, and partially by stress induced deformation during growth. The latter was evident from the facts that: (i) interface vibration, which usually results from misalignment, was not seen during growth; (ii) the onset of buckling occurred only when the ribbon width was $\gtrsim$1.5 cm (i.e., when the thermal stress was sufficiently large); and (iii) the buckled shape appears to be similar to the stress-induced buckles observed previously (e.g., Fig. 7(a) of Ref. 1) with the ribbon being "longer" in a central longitudinal section than along the edges. The residual stresses in the current buckled ribbons were much lower, however, than those grown using the cooling blocks alone,[4] or those grown in a cold radiative environment.[1]

In Run No. 14-205, a second heating element was inserted into the afterheater; this caused a more gradual decrease in the vertical temperature profile. Figures 11 and 12 show typical measured profiles in

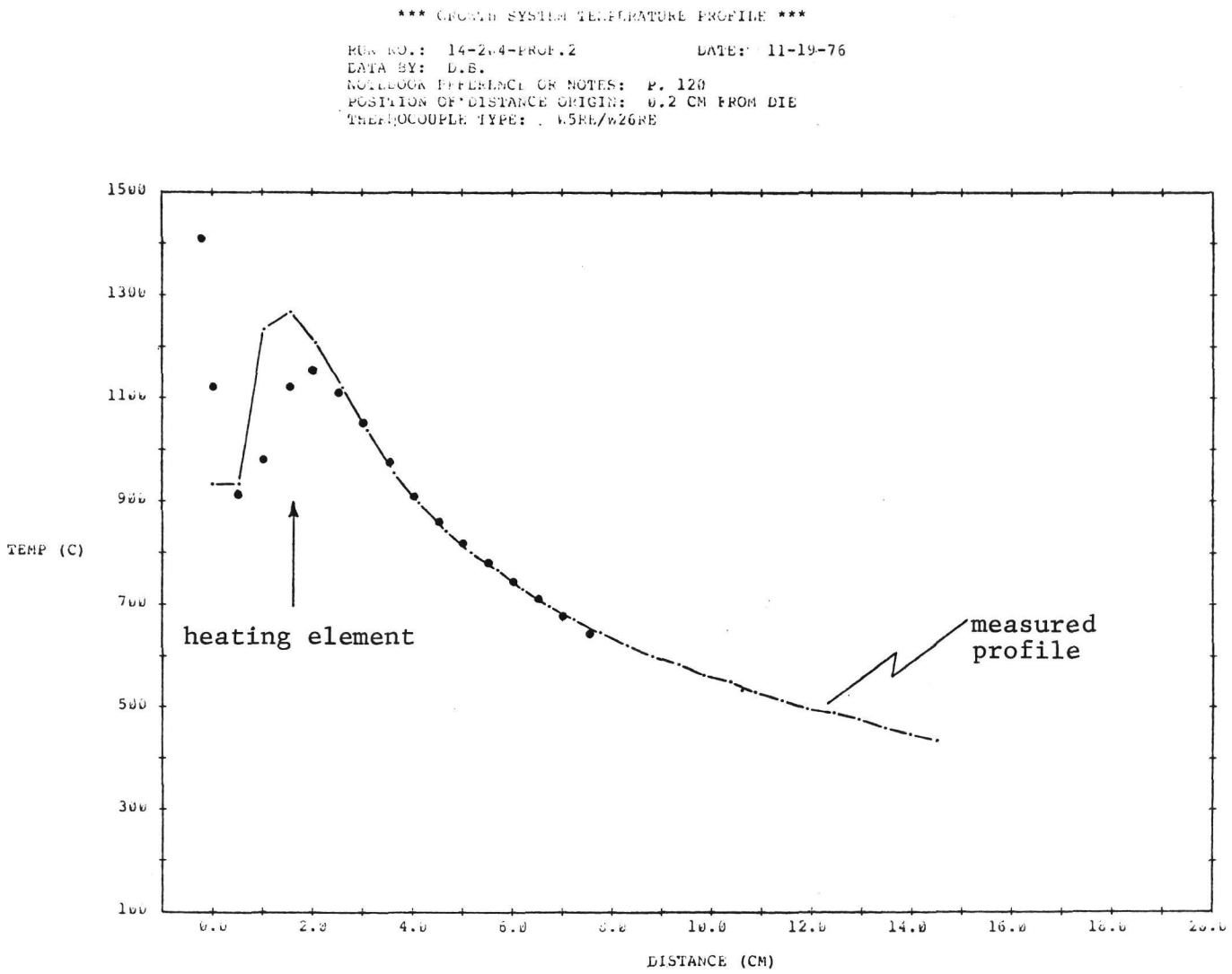

Fig. 11. Measured profile and calculated temperature profile in ribbon (solid points) in Run No. 14-204. The cold block temperature is ~500°C.

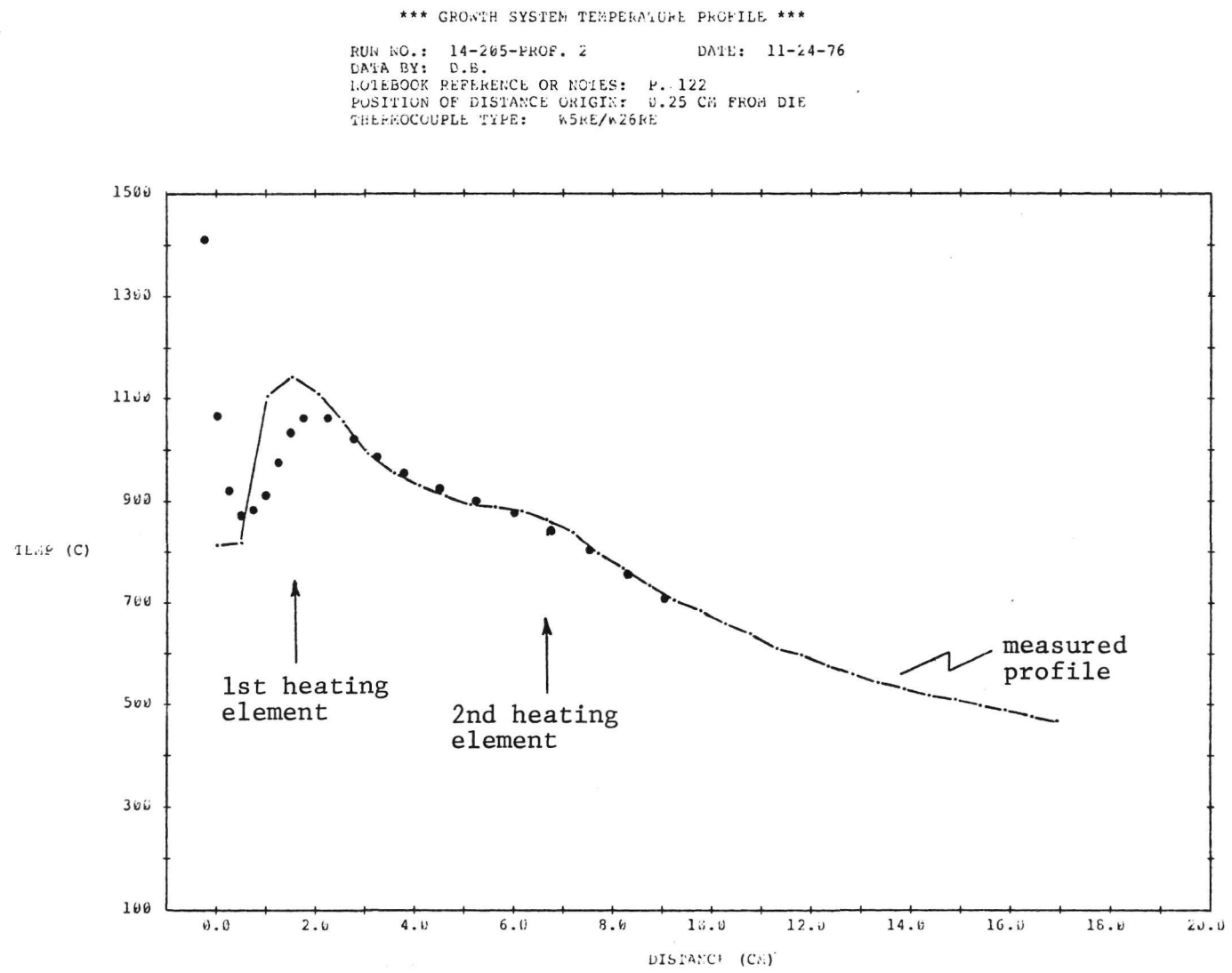

Fig. 12. Measured profile and calculated temperature profile in ribbon in Run No. 14-205. The cold block temperature is ~500°C.

Runs 14-204 and 14-205, respectively. The power in the afterheater is adjusted to give ~1250°C at the hottest point in the afterheater in 14-204 and ~1150°C in 14-205; the figures also show the theoretically calculated profiles in the ribbon.

Several long, nearly full-width ribbons were grown in Run No. 14-205 at rates between 5 cm/min and 6.8 cm/min; the ribbons were excessively buckled when the width was $\gtrsim$1.5 cm. Examination of the buckled shape following growth showed that the buckles were definitely a result of stress-induced deformation during growth. In spite of the buckled shape, however, there was no residual stress in the ribbons as evidenced by scribing and splitting.

The following conclusions can be drawn from these experiments on the effects of the vertical temperature profile on growth rate and residual stress:

(a) As expected, a growth rate of ~7.5 cm/min can be readily achieved with a simple device which provides radiative/convective cooling in the vicinity of the growth interface. In the present experiments, cooling occurred mainly by radiation because of the large spacing between the cooling blocks. The experimental growth rates are consistent with the theoretically predicted maximum rates from profiles such as in Figs. 11 and 12.

(b) It now appears that it will not be necessary for the afterheater to be exactly linear, as long as the temperature decrease to below ~600°C is fairly gradual. Thus, the afterheater profile in 14-204 drops off too rapidly, whereas that in 14-205 is acceptable. (The actual, i.e., calculated, profile in the ribbon follows the thermocouple trace in 14-204, but the "bump" caused by the second heating element in 14-205 is somewhat smoothed out - see Figs. 11 and 12). In both cases, the ribbon is reheated to ~1100°C at the hottest point, where all the stress is likely to be relieved. However, cooling the ribbon as in 14-204 caused further plastic flow and residual stress in the ribbon at room temperature; the more gradual cooling 14-205 leaves the ribbon relatively stress free.

(c) The source of the buckles is of obvious concern, even though some of the buckled ribbon (e.g., in 14-205) was free of residual stress. As seen in the calculated profiles in Figs. 11 and 12, the ribbon is cooled to ~900°C as it passes through the radiation and cooling regions (cf. Fig. 8) before its temperature is raised to ~1100°C again. In the region where the curvature of the profile is reversed (i.e., $d^2T/dz^2 < 0$),

the thermal stresses also act in a reversed manner. Thus, a center longitudinal section is under compression while the outer edges are in tension.[1] Since the ribbon is already longer in the central section, as a result of plastic flow caused by thermal stress in the initial cool-down region (where $d^2T/dz^2 > 0$), the ribbon buckles in the reverse-stress region. Reheating to ~1100°C can relieve the residual stress, but it cannot relieve the permanent buckles in the ribbon.

(d) The above considerations suggest that a cooling/reheating profile in the ribbon, as in Figs. 11 and 12, should be avoided. This may be achieved by a narrower cooling zone such that the ribbon temperature does not decrease below 1100°C. Alternatively, the afterheater may be operated at a lower temperature (at its hottest point) to decrease (or eliminate) the reheating in the ribbon. The former technique may involve a trade-off with the attainable growth rate, the latter with increased residual stress in the ribbon. Another possible solution may be to decrease the rate of reheating (i.e., the reverse curvature in the profile) by moving the afterheater further away from the die.

Experimental work along the above lines will continue during the next and subsequent quarters. Theoretical work will be carried out to find the optimum combination of the various parameters in the cooling/afterheater unit of the cartridge to give the desired growth rate and temperature profile. The optimization will be carried out near the measured values of the parameters rather than the assumed values used in earlier calculations (cf. Tables III to V). For example, typical cold-block temperatures (i.e., T_C) in the cartridge have been observed to be ~700°C to ~900°C; this probably accounts for the fact that helium gas had to be used in the experiments on JPL No. 1 to attain growth rates >5 cm/min.

D. System and Ribbon Purity

The molybdenum used for station parts is not very clean (Table VII). To thoroughly clean the surfaces of new molybdenum components, a sulfuric acid bath treatment and vacuum bakeout will be used before they are introduced into the growth system. Both tungsten and molybdenum are readily oxidized by CO and CO_2 as well as by O_2 and H_2O. Oxidation of molybdenum station components occurs during every run (Fig. 13). Most of the molybdenum oxide on hot zone components is removed by reduction and transport in a 95% Ar 5% H_2 atmosphere just prior to shutdown.

In the interest of purity the system has been purged of alumina

Table VII. Molybdenum Analysis - Supplied by the Manufacturer

ELEMENT	GUARANTEED ANALYSIS	TYPICAL ANALYSIS
Molybdenum	99.93%	99.96%
Carbon	30 PPM Max.	15 PPM
Oxygen	50 PPM Max.	30 PPM
Hydrogen	20 PPM Max.	10 PPM
Nitrogen	10 PPM Max.	5 PPM
Iron	70 PPM Max.	50 PPM
Nickel	10 PPM Max.	2 PPM
Copper	20 PPM Max.	8 PPM
Lead	10 PPM Max.	<5 PPM
Zinc	10 PPM Max.	3 PPM
Silver	10 PPM Max.	<5 PPM
Aluminum	20 PPM Max.	8 PPM
Silicon	30 PPM Max.	<30 PPM
Sodium	30 PPM Max.	10 PPM
Potassium	20 PPM Max.	5 PPM
Calcium	20 PPM Max.	6 PPM
Barium	20 PPM Max.	<20 PPM
Phosphorous	30 PPM Max.	10 PPM
Manganese	5 PPM Max.	2 PPM
Magnesium	10 PPM Max.	<5 PPM
Cobalt	10 PPM Max.	3 PPM

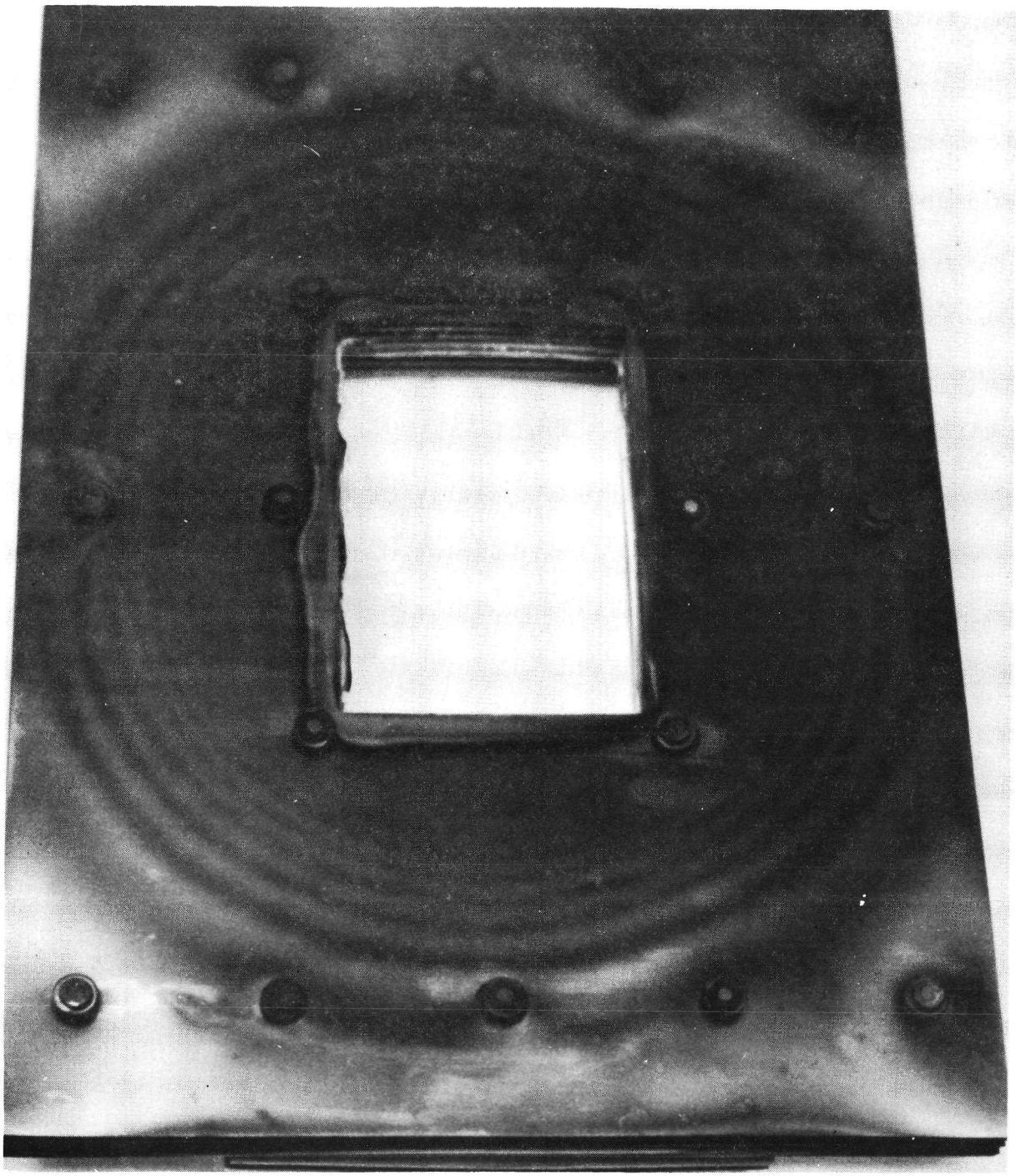

Fig. 13. Top heat shield pack showing oxidation.

components. For the first few runs alumina was used to space the main heater power studs from the bottom of the heat shield package, to space some of the elements of the die holder cartridge, and as thermocouple protection tubing. In every case, the alumina components have been replaced with quartz in an effort to reduce aluminum migration to the melt or growing ribbon.

A high temperature halogen purification process for graphite components was established under a previous contract, but the capacity of the bakeout system has been limited. An expanded bakeout system capable of cleaning large graphite parts including the main heating elements (Fig. 14) and crucible holder from the growth system JPL No. 1 is now in operation. All graphite parts will now be purified prior to use in growth processes.

Finally, handling procedures are being improved. More care is being taken in the storage of components and during the assembly of components. It is hoped that the introduction of the above processing procedures will result in silicon ribbon containing fewer impurities and, therefore, providing far more efficient solar cells.

Beyond measurements of dimension and stress, the initial characterization of each ribbon grown in JPL No. 1 includes IR transmission scans. For ribbons of the same resistivity, substantial absorption of infrared between about 7 and 25 or 30 microns is taken as an indication of the existence of electrically detrimental impurities (hence, free carriers). The IR scan also serves as an indicator of the character of any surface film on the newly grown ribbon. Oxygen and silicon carbide peaks are observed at 9 and 12½ microns, respectively. Samples with absorption peaks are usually etched and scanned again to determine whether the oxygen and carbide are in fact on the surface or in the bulk. Typical scans of ribbons from the JPL No. 1 furnace are seen in Fig. 15.

IR transmission scans of ribbons 18-6 and 18-7 were made. The trace of ribbon 18-6 is shown in Fig. 16 and is the same as that of 18-7. This flat trace is typical of material doped to 10 $\Omega \cdot cm$ and can be compared to traces of 1 $\Omega \cdot cm$ earlier material.

The absence of oxide or SiC peaks is significant. It indicates the absence of the surface films typical of "rf" grown EFG silicon ribbon.

Spots of surface film are observed to form on the ribbon whenever it is held stationary for any substantial amount of time in front of the helium inlets in the cartridge (Fig. 17(c)). It was feared that some impurities in the cooling gas were reacting with the ribbon surface; the

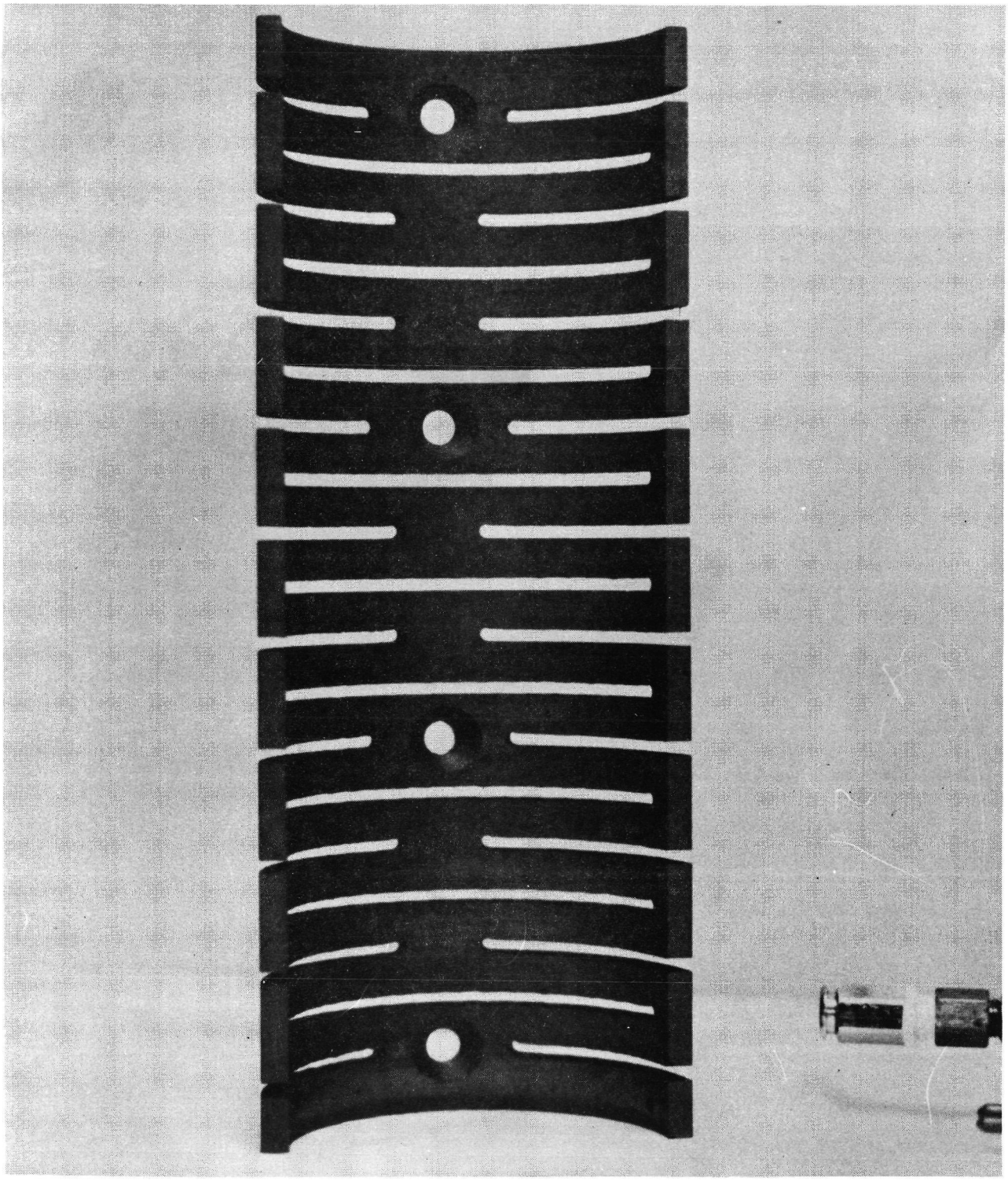

Fig. 14. Main zone heating element.

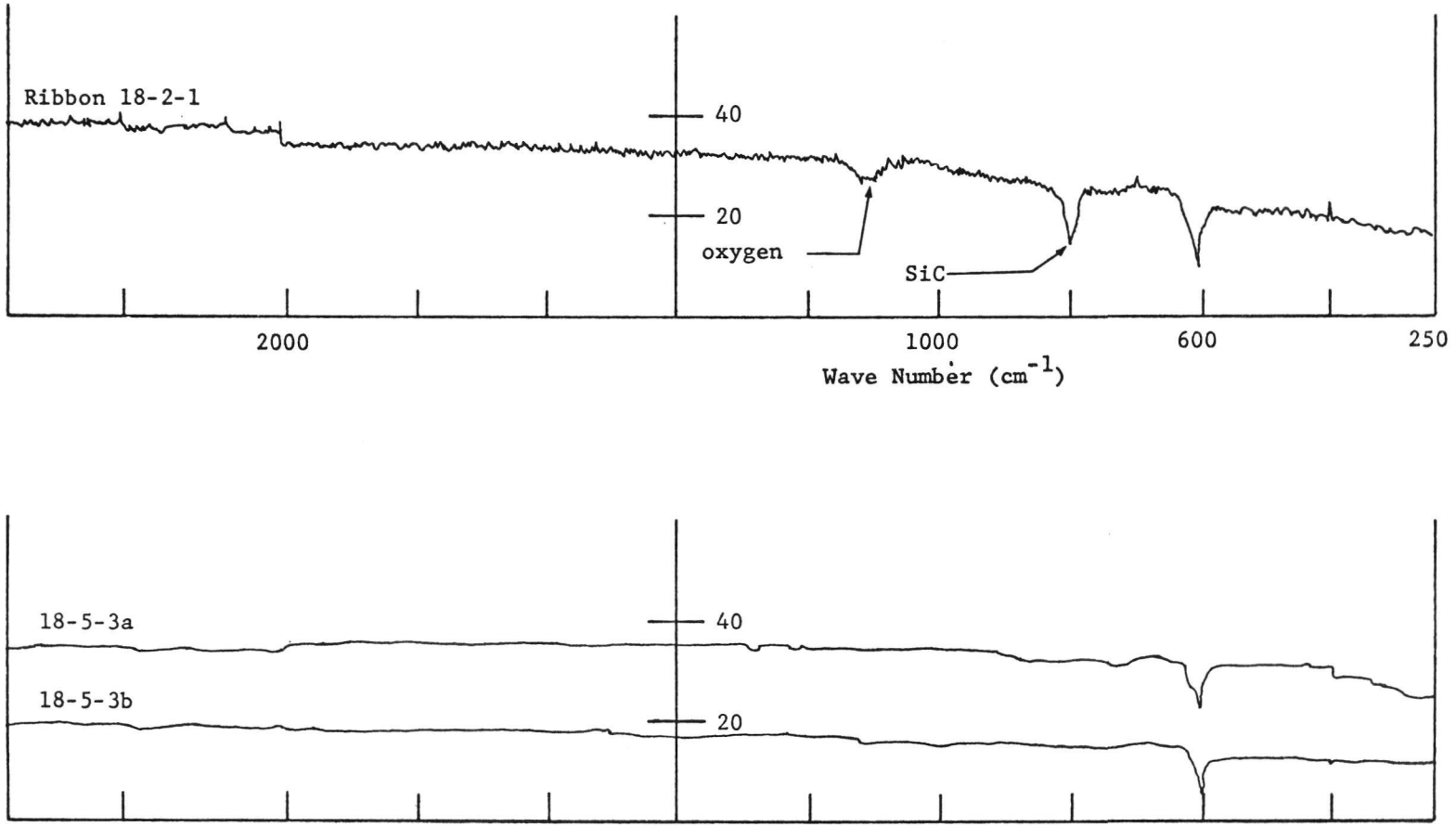

Fig. 15. IR absorption traces of ribbons 18-2-1 and 18-5-3. Note the absence of SiC film in ribbon 18-5-3.

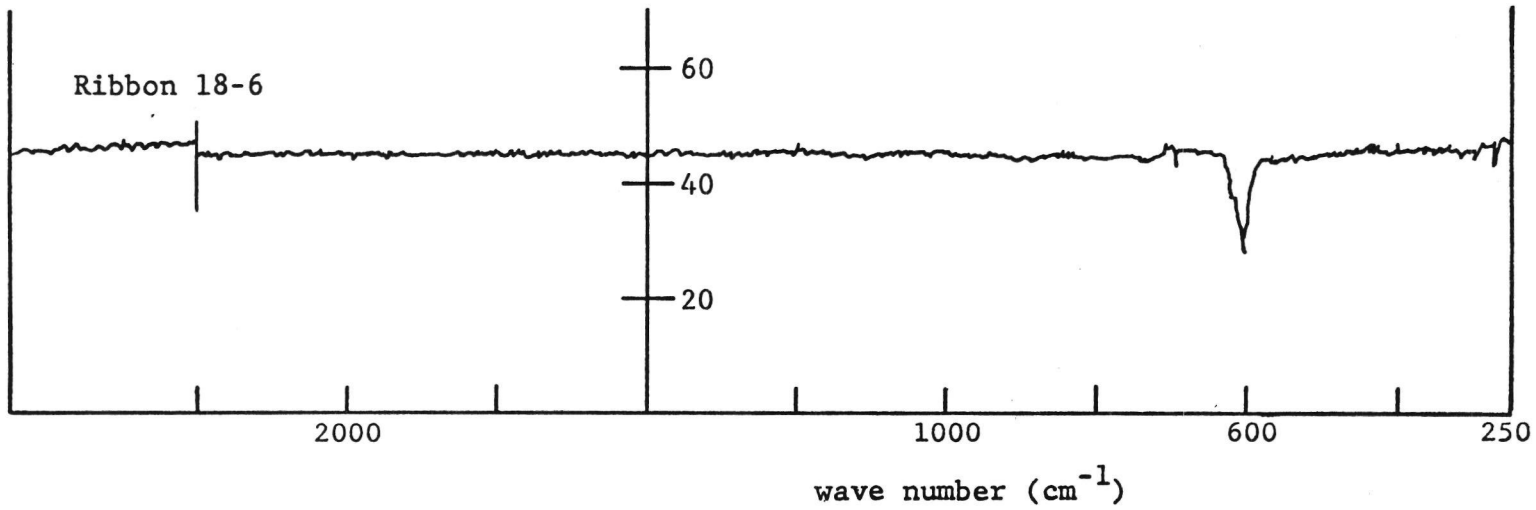

Fig. 16. IR transmission scan of ribbon 18-6 (JPL No. 1).

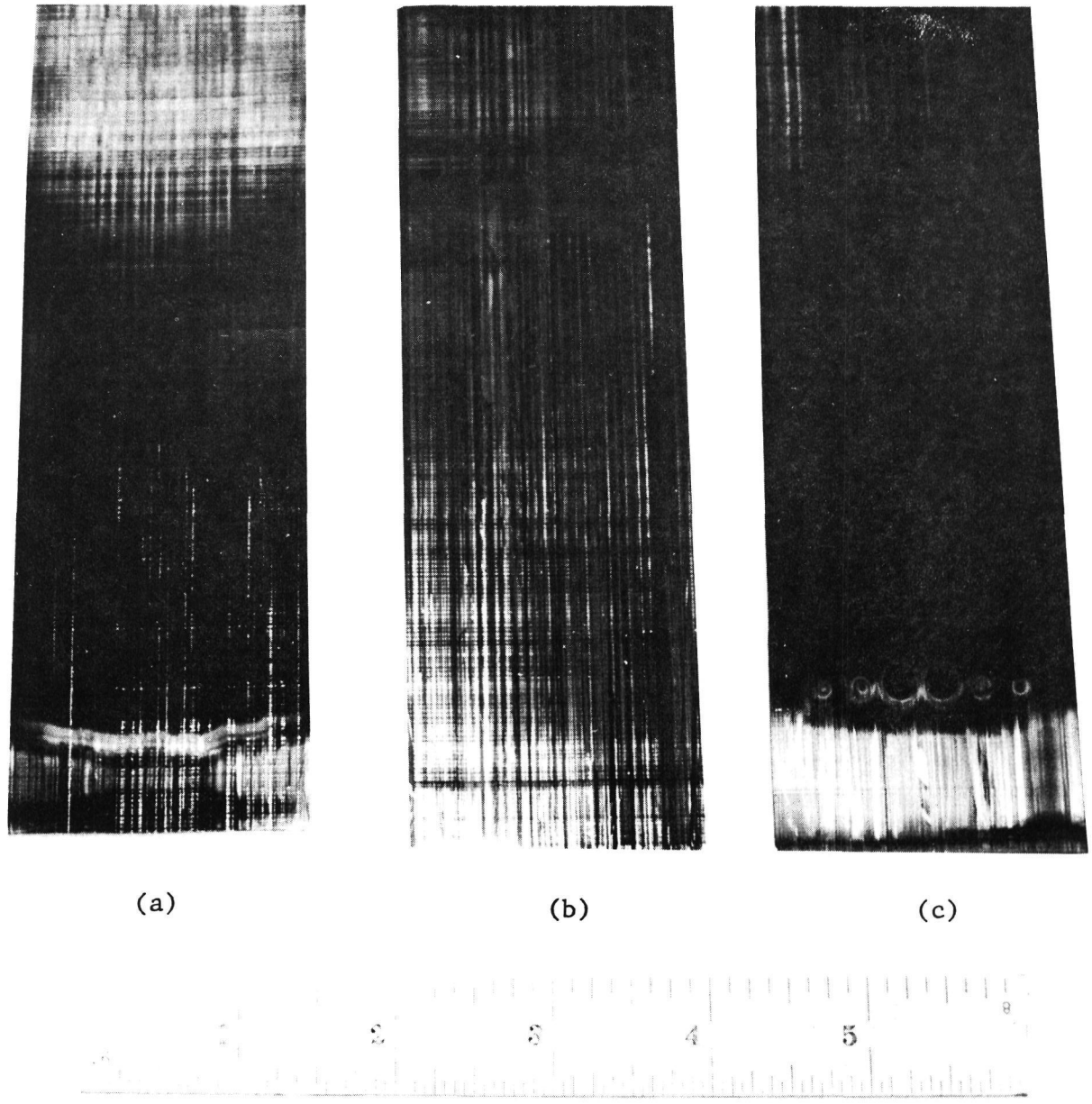

Fig. 17. 5 cm wide ribbons. (a) Showing oxide band ~15 mm from ribbon end. (c) Showing oxide spots which formed opposite helium ports in cartridge.

extended time allowed enough reaction to take place to be noticeable. However, IR scans before and after etching showed the films to be oxide and SiC. As mentioned previously, there is always a substantial amount of SiO vapor in the system. Fig. 18 shows SiO vapor swirling up past the die and out under the cartridge floor just after the cartridge was lifted free of the hot zone. This heavy smoke is visible in every run just before the die is dipped and just after it is pulled free. Fig. 19 shows the die suspended over the top shield opening at the end of a run. Note the oxide deposits hanging between the shield package and the die. (The side-slotted die is cracked by the expanding silicon on cool down). This material is occasionally seen to fall into the melt early in a run. Deposits are seen on the outside of the cartridge in Fig. 20 and between shield layers in Fig. 21.

A sample of the heavy cream colored deposit was taken from the top shield pack after Run 18-5. For this run, all system components except graphite heating element and crucible holder had been thoroughly cleaned; e.g., washed, etched, or baked out. The sample was analyzed in a bismuth oxide buffer by emission spectrography against standards also in bismuth oxide for calibration. The results (Table VIII) indicate very high iron and aluminum concentrations; it is possible that the oxide deposits may be the prime source of active impurities carried into the melt. Samples of these deposits from an all-baked-out system are now being analyzed. A simple gas flushing system intended to remove the oxides and suboxides as they formed was ineffective. Alternatives are described under Plans later in this report.

The electronic properties of the ribbons depend upon purity and impurity distribution. Resistivity, mobility and carrier concentrations for various ribbons are given in Table IX.

E. Structure and Related Electronic Properties

It has been previously reported, based on EBIC data and examination of small area mesa diodes, that SiC particles, intersecting boundaries and low angle grain boundaries are detrimental to solar cell performance because of localized recombination effects in the vicinity of these defects.[1]

In order to ascertain the relative contributions of the space charge region and the bulk of a solar cell to the recombination contrast observed in the EBIC mode, Schottky barrier devices were examined in this mode of operation and by varying the depth of penetration of the incident electron beam by changing the electron accelerating voltage. In Fig. 22

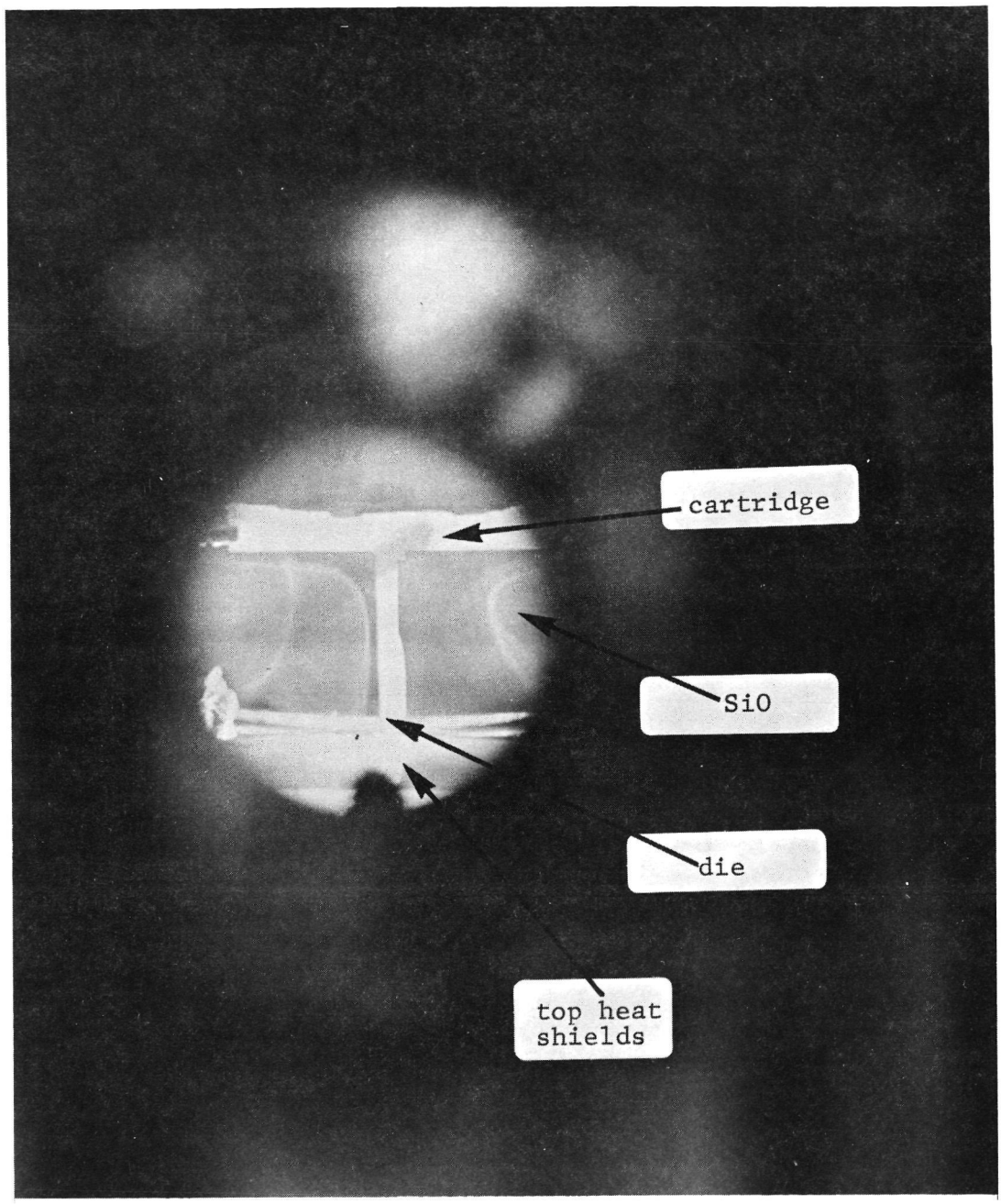

Fig. 18. SiO vapor swirls up out of the hot zone to the left and right of the cooling die (view from the door port during the shutdown process).

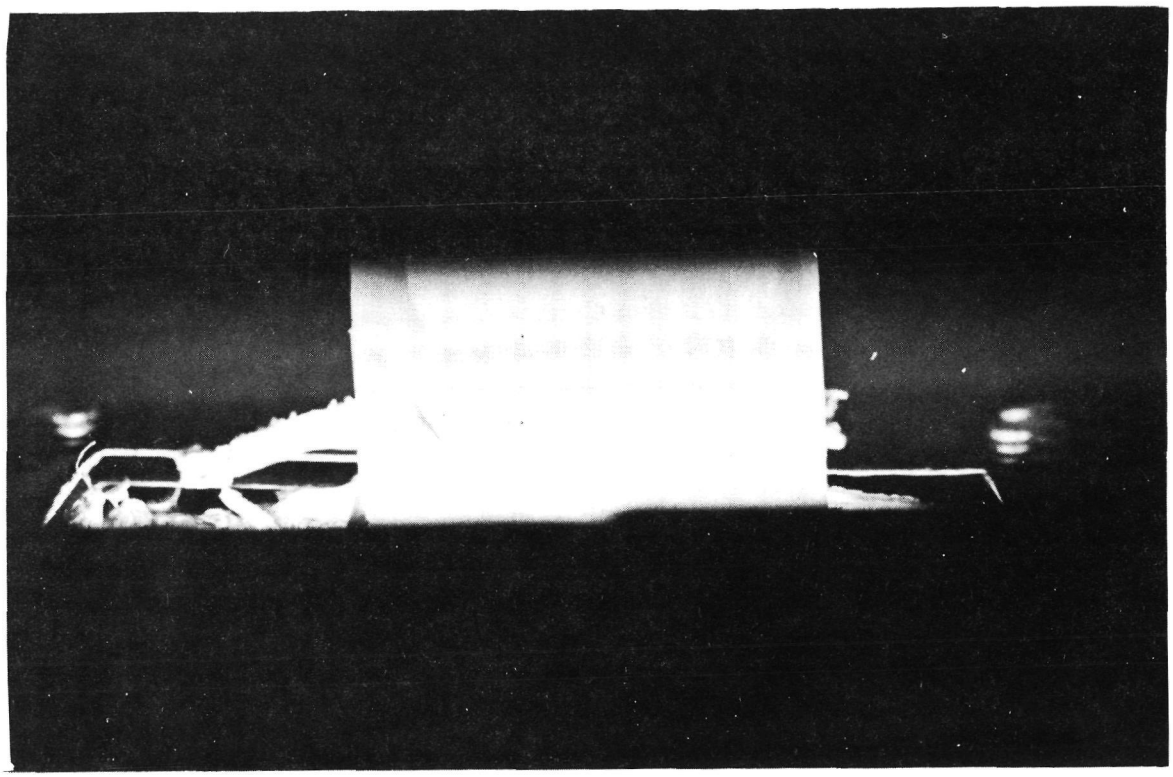

Fig. 19. Heavy oxide deposits are seen suspended between the elevated die and the molybdenum heat shield pack. Some oxide fell into the melt when the die was further withdrawn. (The molten silicon expanded on freezing causing the crack seen in the edge of the side-slotted graphite die).

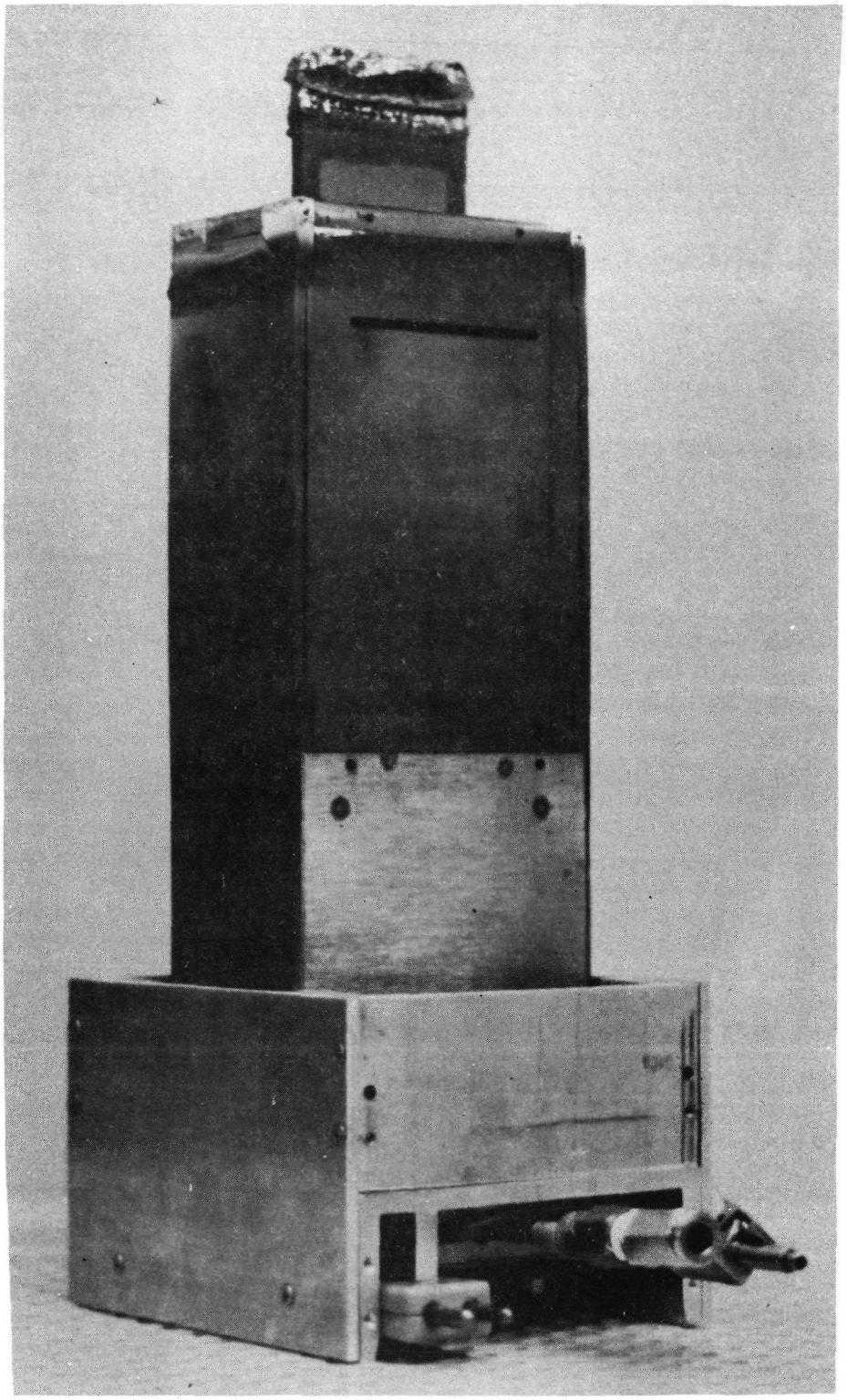

Fig. 20. A die-holding cartridge after a run. Frozen silicon is seen on the die and condensed oxides around the viewports.

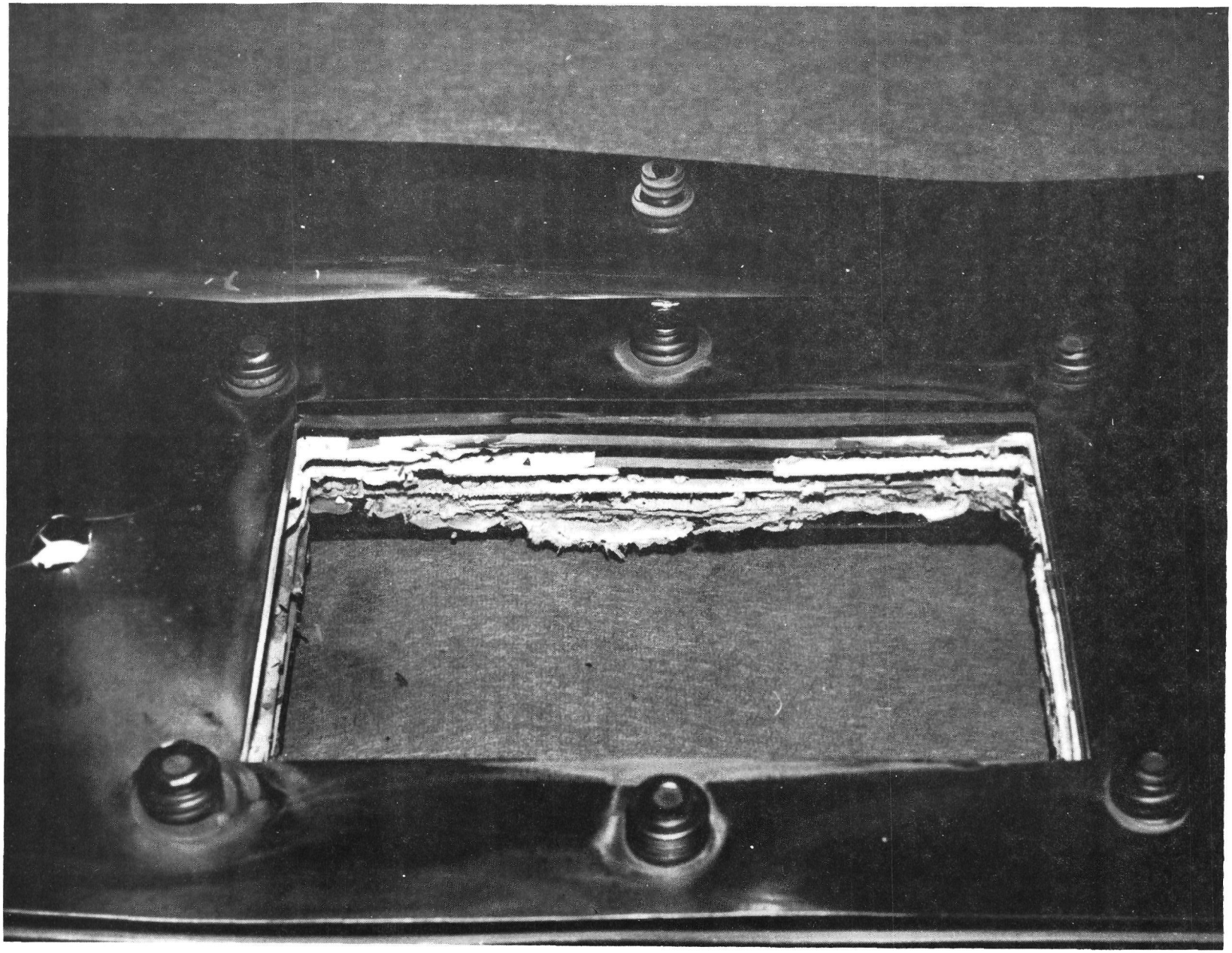

Fig. 21. Loose oxide deposits fill the inner edge of the top shield pack after a growth run is completed.

Table VIII. Emission Spectrographic Analysis* of SiO Deposits in the Molybdenum Heat Shields of JPL No. 1 (Run 18-5)

Fe	100 - 1000 ppm
Mo	30 - 300 ppm
Al	10 - 100 ppm
Ni	3 - 30 ppm
CaCr	1 - 10 ppm
Mg	.3 - 3 ppm
Cu	.1 - 1 ppm

*This data is from a system in which the graphite crucible holder and the heating element were not subjected to a high temperature halogen treatment. Consequently, these graphite components could be source of the Fe, Cu, etc., in the 'SiO' deposit.

Table IX. Electronic Characterization

SAMPLE NO.	RESISTIVITY ($\Omega \cdot cm$)	MOBILITY ($cm^2/V\text{-}sec.$)	CARRIER CONCENTRATION (cm^{-3})
18-3	0.67	185	5×10^{16}
18-4-4	1.10	226	2.51×10^{16}
18-4-5	1.03	199	3.06×10^{16}
18-4-6	1.08	176	3.30×10^{16}
18-4-6	0.89	238	2.97×10^{16}
18-5-1	0.84	217	3.45×10^{16}
18-5-2 (C)	0.72	193	4.51×10^{16}
18-5-3 (C)	0.72	239	3.62×10^{16}
18-6	5.01	244.1	5.11×10^{16}
18-4-2 #1	1.0	230	2.9×10^{16}
18-4-2 #2	0.8	268	2.8×10^{16}
18-8-4 #1	1.4	187	2.3×10^{16}
18-8-4 #11	1.4	199	2.3×10^{16}

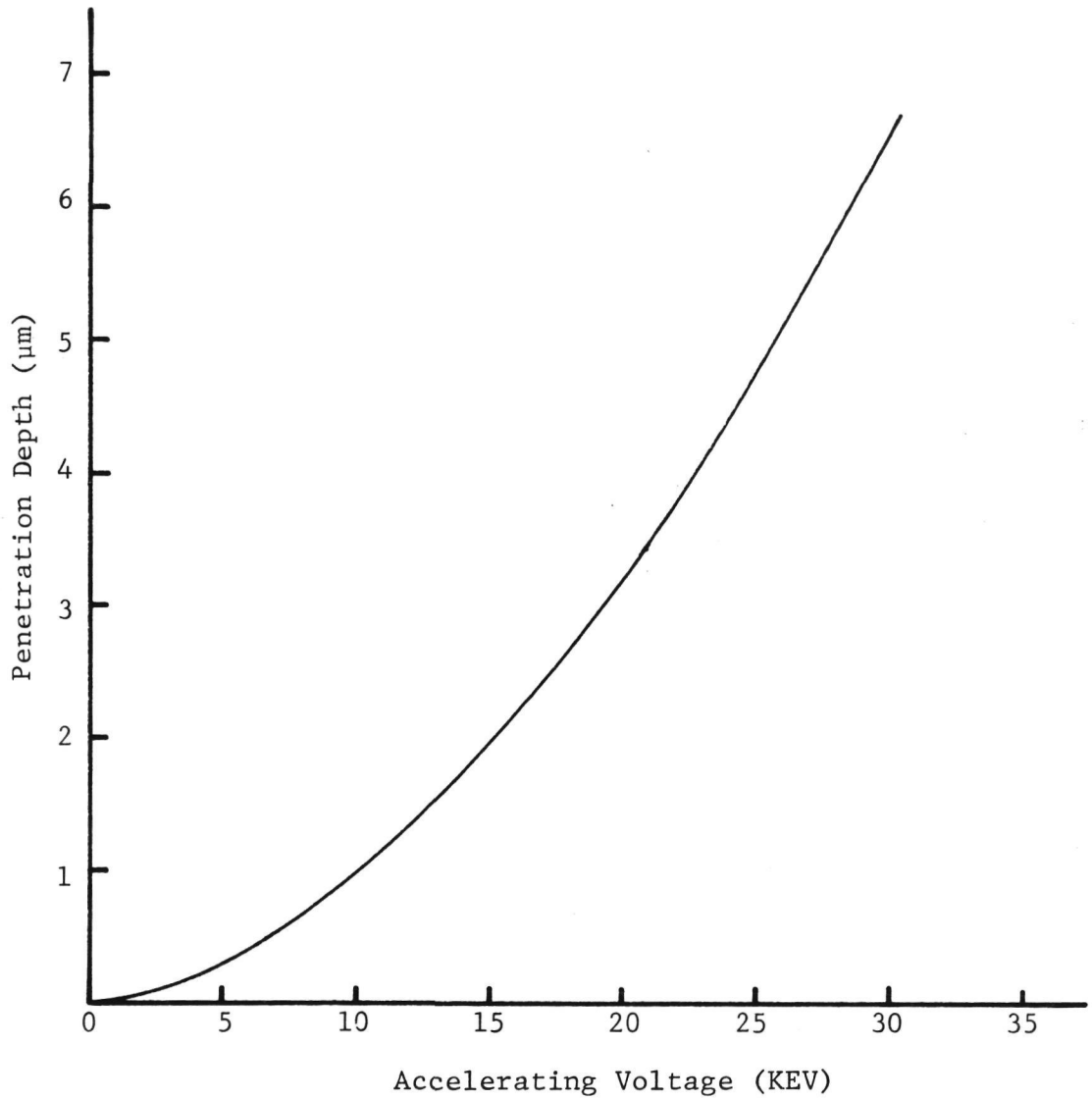

Fig. 22. Electron beam penetration depth as a function of accelerating voltage.

we plot the maximum electron beam penetration depth as a function of accelerating voltage. The calculations are based on Everhart and Hoff's[5] data, and represent, to a good approximation, the depth to which electron-hole pairs are generated in the bulk of the semiconductor. Fig. 23 shows EBIC images obtained on a Schottky barrier device at accelerating voltages of 30, 25, 20, 15 and 10 KEV. These correspond to beam penetration depths of approximately 6.6, 4.8, 3.2, 2.0, and 1.0 microns respectively. Notice that the degree of recombination at the boundaries decreasing as the accelerating voltage decreases. In fact, the recombination contrast at boundaries and at dislocations is extremely low at 10 KEV, i.e., at a penetration depth of 1.0 μm.

The Schottky barrier was fabricated by evaporating 500 Å of aluminum on 1 Ω·cm ribbon samples. Assuming a junction built-in voltage of 0.4 V and a base carrier concentration of 10^{16} atoms/cm^3, the space charge region width is found to be approximately 0.23 μm at zero-bias conditions.[6] Thus, even at 10 KEV, the electron beam completely encloses the space-charge region. Increasing beam penetration results in progressively more of the base region being enclosed in the beam. The increase in contrast at greater depths of penetration thus should be arising from defects present in the bulk of the base material. The width of a feature in the EBIC images will depend on the inclination of the defect with respect to the specimen surface. A defect which is normal to the sample surface (and hence, parallel to the electron beam) will not exhibit a change in width as the beam penetration changes (assuming a homogeneously decorated defect through the bulk). Since beam penetration is proportional to $(\xi)^{1.75}$, where ξ is the accelerating voltage, a plot of the width of the recombination zone at a defect against $(\xi)^{1.75}$ should yield a straight line. Such a plot is shown in Fig. 24 for two linear boundaries observed in Fig. 23. It is quite evident from the plot that in EFG silicon, where crystallographic defects extend through the thickness of the ribbon, space charge recombination-generation effects contribute minimally to the total observed recombination, and that the predominant recombination effects are associated with the local space charge regions associated with the electrically active defects.

F. Intensity Effects on Recombination at Defects

Measurement of diffusion lengths in solar cells is made routinely under essentially 'dark' conditions. However, a solar cell operates under 1 sun condition, corresponding to a photon flux of approximately 10^{16} photons/cm^2/sec. Under 'illuminated' conditions, the device is

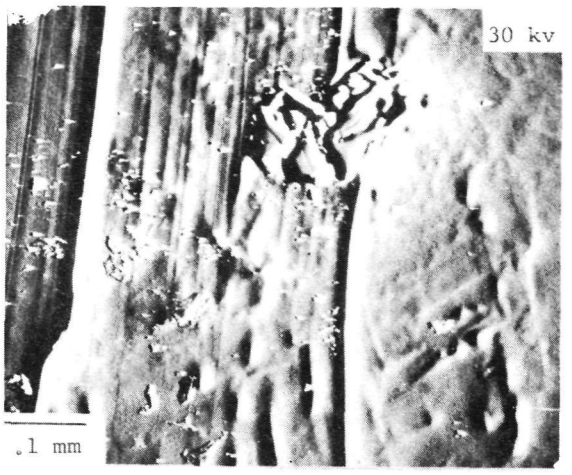

(a)

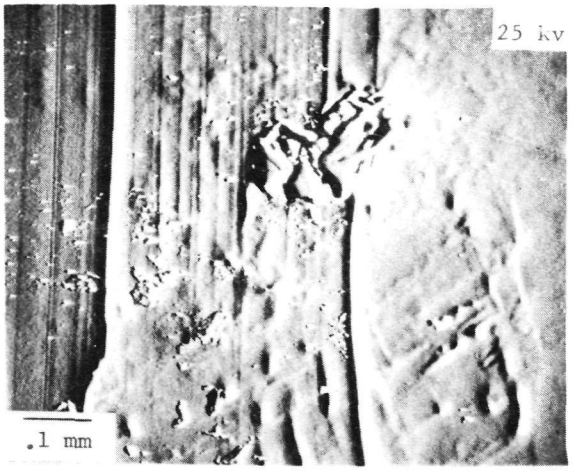

(b)

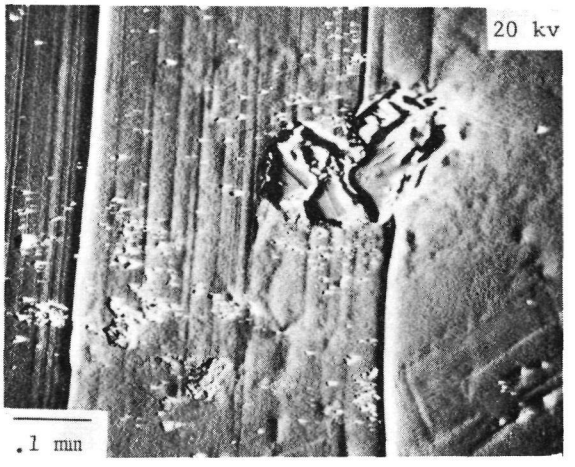

(c)

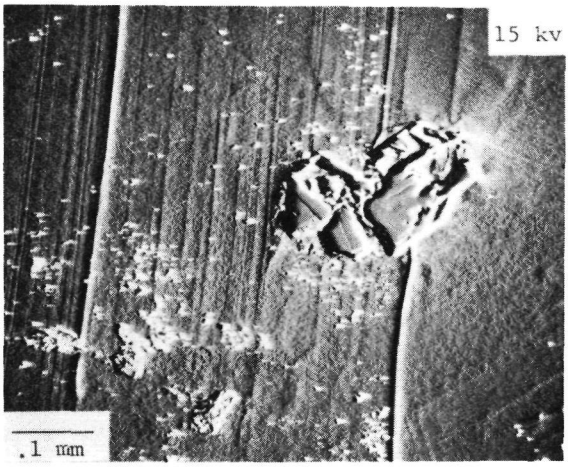

(d)

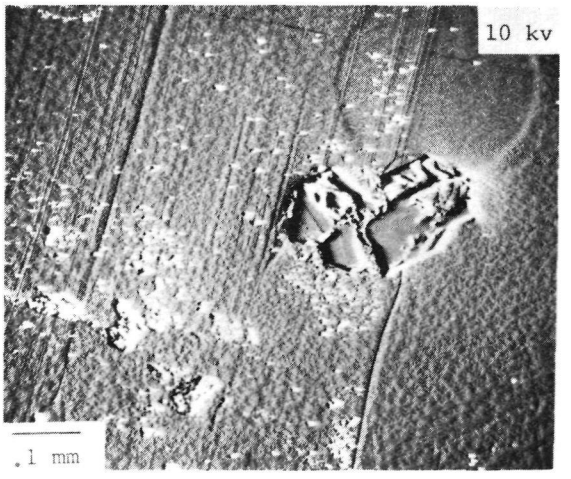

(e)

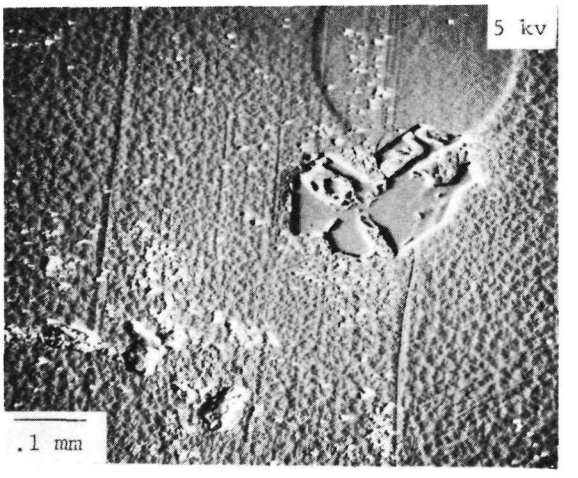

(f)

Fig. 23. Schottky barrier EBIC as a function of accelerating voltage (i.e., penetration depth). Note the decrease in width of recombination zone as the penetration depth decreases.

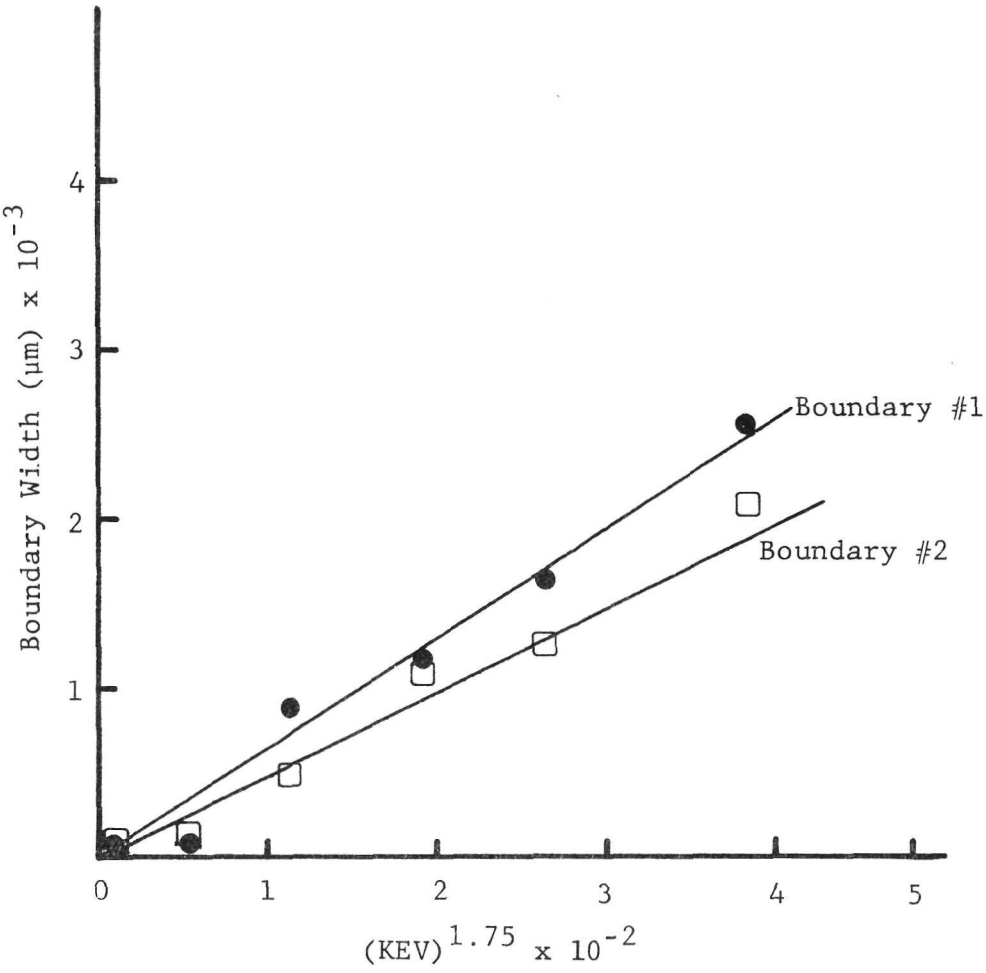

Fig. 24. The width of the recombination zone at a defect as a function of accelerating voltage.

operating in a forward bias mode. Such forward biasing will lead to:

(a) A decrease in the space charge region width, resulting in a smaller fraction of the defect being enclosed in the space-charge region.

(b) Trap saturation in the material, resulting in lower recombination.

In order to simulate the 'illumination'conditions seen by a solar cell under normal operation, EBIC data was gathered on a section of a solar cell in the 'dark' condition and under illumination by incorporating a tungsten light bulb in the specimen chamber of the SEM. The forward biasing obtained by optical illumination was 0.11 V. Fig. 25(a) shows an EBIC image obtained in the 'dark' and Fig. 25(b) shows the EBIC image of the same area under illumination. In Fig. 25(c) we show an EBIC image wherein the left-hand portion was taken in the 'dark', while the right-hand half of the picture was taken under illumination. Notice the distinct decrease in recombination contrast on forward biasing during illumination.

The width of the space charge region can be written as:[6]

$$Z_D = \sqrt{\frac{2K_s E_o}{q\ N_A}\ (V_b + V_{ext})}$$

where K_s = dielectric constant
E_o = permittivity of free space
q = electron charge
N_A = base concentration
V_b = barrier height, and
V_{ext} = applied external bias.

Thus, the external bias changes Z_D by a very small fraction, and for a forward bias of 0.11 V, the change in space-charge width is calculated to be only 0.04 μm. The changes in recombination contrast, therefore, cannot be entirely attributed to a decrease in the volume of defect being enclosed in the space-charge region.

Saturation of the available traps, therefore, seems to be a plausible explanation of the phenomenon observed in the material. The above contention seems to be borne out by observations of changes in diffusion length, estimated from spectral response measurements, as a function of incident photon intensity.[7] Figure 26 shows a plot of diffusion length measured as a function of photon flux, with the flux varying from 0 to approximately 10^{16} photons/cm^2/sec at 1 sun intensity. The nature of the traps can be further investigated by employing radiation with wavelengths

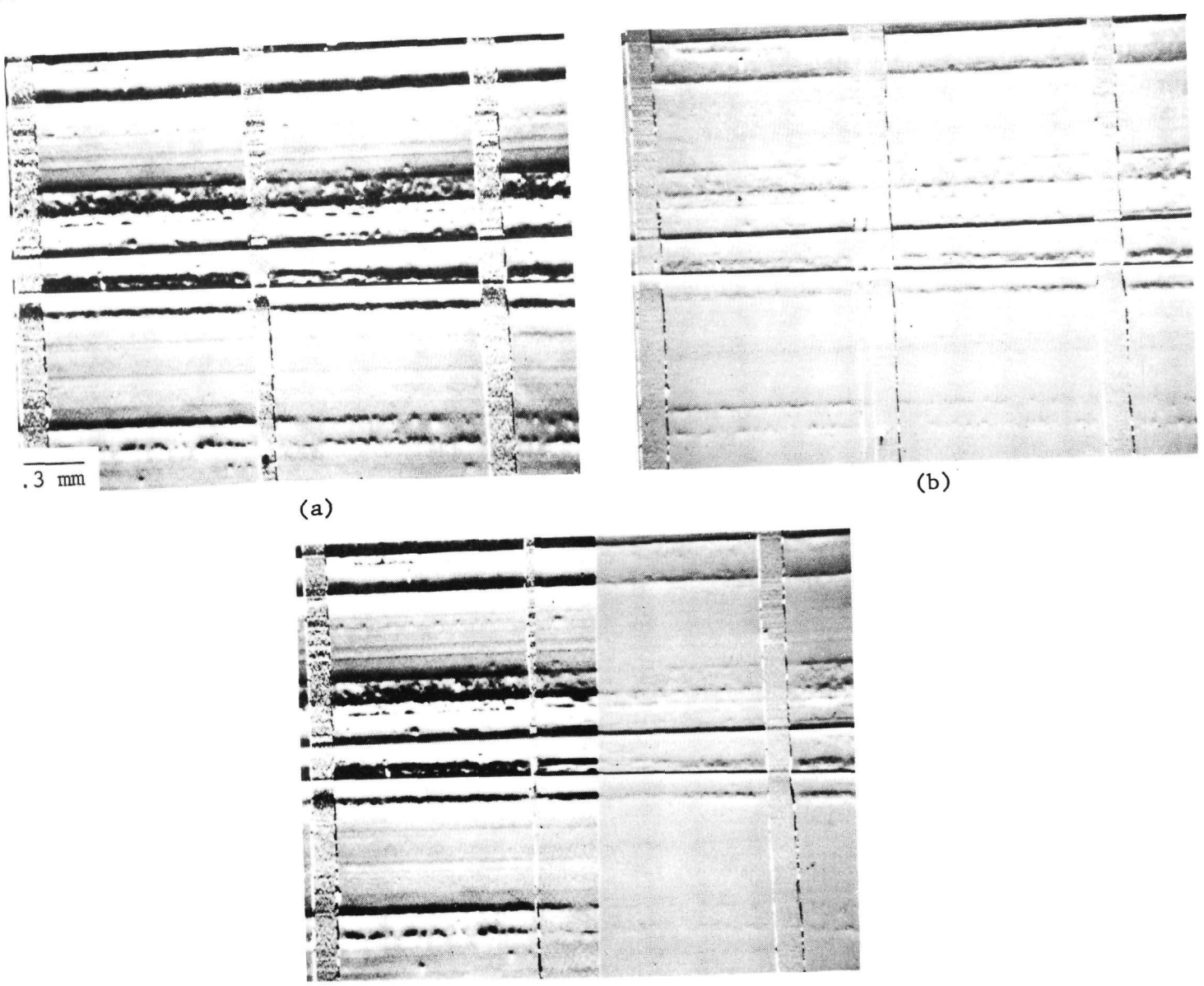

Fig. 25. Effect of illumination on recombination at crystallographic defects.

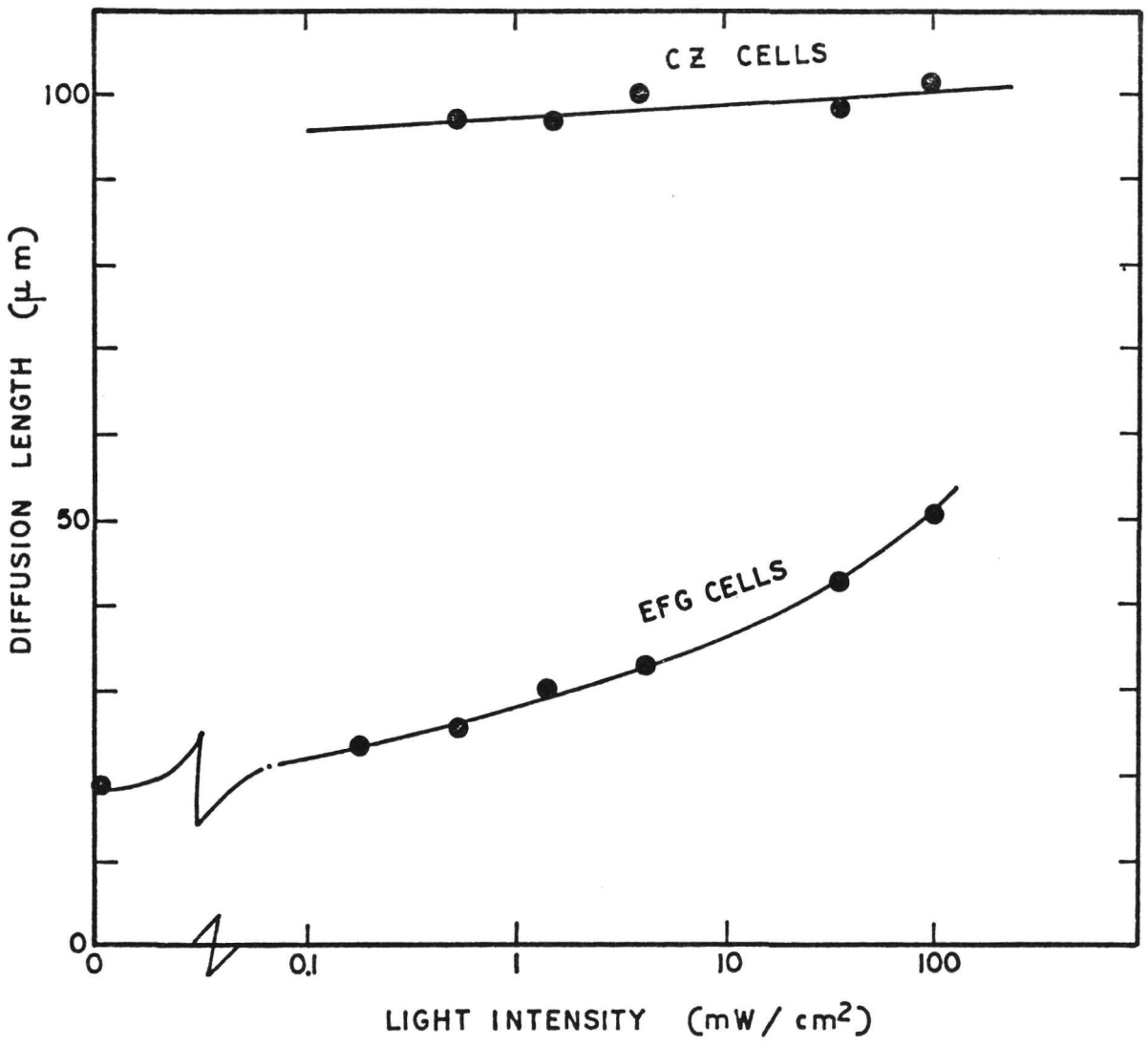

Fig. 26. Diffusion length as a function of photon flux.

corresponding to the bandgap in silicon, and such investigations are underway at the present time.

G. Problems

None.

H. Plans

Having established that 5 cm wide ribbon can be grown at rates up to 5 cm/minute with no residual stress, it is planned to intensify the effort in the quality aspects of ribbon growth.

Some of the machine related parameters that are considered to affect ribbon quality include the following:

(a) The influence of contaminated SiO deposits which can fall into the crucible; as shown elsewhere in this report preliminary chemical analysis of "SiO" deposits on the molybdenum insulation in the furnace indicates that these deposits contain significant quantities of iron, molybdenum and other metallic elements. These deposits can be detached from the various interior surfaces of the furnace and fall into the silicon melt.

(b) Since the furnace is relatively open during the course of introduction of the cartridge into the chamber there exists the possibility that atmospheric contaminants can enter the chamber and contaminate the melt even though a high rate of argon flow is maintained throughout the process.

(c) A third possibility relates to the configuration and components of the cartridge. The cartridge is a relatively complicated piece of apparatus containing a variety of graphite, molybdenum, and stainless steel components with a number of close fitting parts arranged in a small volume. As a consequence three aspects of the cartridge need to be examined for their possible influence on melt and crystal contamination. (i) Contaminants from the components of the cartridge can enter the melt or the ribbon; the graphite parts of the cartridge are all subjected to high temperature halogen treatments and as a consequence should be sufficiently free of impurities. The stainless steel and molybdenum parts may introduce impurities if they attain sufficiently high temperatures. It is yet to be determined whether this is an important effect. (ii) Since the cartridge is not "pumped out" and purged with argon prior to its introduction into the chamber, trapped air and atmospheric contaminants can be introduced into the growth chamber. This effect is probably magnified as a result of the complex nature of the cartridge. (iii) The

possibility exists for SiO buildup within the cartridge as a result of the tightly packed interior of the cartridge. Local accumulation of SiO deposits among the components of the cartridge can result in spalling or detachment of the SiO and the resulting contamination of the melt if the SiO is also contaminated.

In order to investigate the possible influence of the above mentioned variables as well as other parameters, the following experiments are planned during the next and subsequent quarters.

(a) In order to prevent possible melt contamination by contaminated SiO it is planned to exercise greater care during the introduction of the cartridge into the furnace chamber. A crucible cover will be designed and evaluated to determine if particulate contamination can be eliminated.

(b) By employing a solid polysilicon charge with a notch provided in it to accommodate the die, it is planned to assemble the furnace with the cartridge in place prior to heat up. This is expected to keep atmospheric contamination out of the system throughout the process.

(c) Further studies of the gas flow conditions in the system will be conducted with a view towards determining the kinetics and dynamics of "SiO" deposition in order to determine whether "SiO" formation and deposition can be influenced.

(d) The influence and the nature of contamination will be examined by employing previously characterized ribbon seeds for growth in order to assess whether contamination is a liquid phase or a solid state phenomenon.

(e) An alternative to the cartridge will be designed and built in order to simplify the system. The new configuration will exclude many of the complex aspects of the cartridge such as die heater, ribbon coolers and the afterheater.

(f) It is planned to conduct a significantly increased amount of chemical analysis of various materials including the silicon charge remaining in the crucible following a growth run, the various deposits that form on the internal surfaces and components of the growth chamber, and an analysis of the grown ribbon. The intention is to attempt to identify the particular contaminants and their sources.

Page Intentionally Left Blank

III. REFERENCES

1. A.D. Morrison et al., "Large Area Silicon Sheet by EFG", Annual Progress Report, ERDA/JPL 954355/76-3 (September, 1976).

2. "Horizontal Configured EFG Machine Model 1 - Standard Operating Procedure", submitted in partial fulfillment of subcontract ERDA/JPL 954355 (June, 1976).

3. D.N. Jewett and B.H. Mackintosh, Mobil Tyco Solar Energy Corporation, unpublished research (1976).

4. A.D. Morrison, et al., "Large Area Silicon Sheet by EFG", Third Quarterly Progress Report, ERDA/JPL 954355/76-8 (June, 1976).

5. T.E. Everhart and P.H. Hoff, J. Appl. Phys. 42, 5837 (1971).

6. S.M. Sze, "Physics of Semiconductor Devices", Wiley - Interscience, London (1969).

7. K.V. Ravi et al., 12th IEEE Photovoltaic Specialists Conference Record (1976) (in print).

Page Intentionally Left Blank

APPENDICES

1. An Updated Program Plan

Table X.

2. Man Hours and Costs

Previous man hours were 5852 and cost plus fixed fee was $180,911. Man hours for October plus November were 1596 and cost plus fee was $50,446. Man hours and cost for December are estimated to be 588 and $22,297 respectively. Therefore, fourth quarter man hours are estimated to be 2184 and cost plus fee to be $73,243. Total cumulative man hours and cost plus fixed fee are estimated to be 8036 and $254,154 respectively.

3. Engineering Drawings and Sketches Generated during the Reporting Period

Figures 27 - 38.

4. Summary of Characterization Data Generated during the Reporting Period

Ribbons have been grown with measured stresses between 0 and >11 K psi. Ribbons grown from JPL No. 1 do not have characteristic surface films. Oxide deposits throughout the growth system contain electrically active species and may be the source of melt impurities. Samples typically have low mobilities 185-268 cm^2/V-sec and L_D too low to measure. Using EBIC, it has been observed that recombination effects around inclusions decrease under illumination. This effect is being studied.

5. Action Items Required by JPL

None.

6. New Technology

During this reporting period, none. Cumulative new technology: heat sinks (Figs. 52 and 53[3]) to promote rapid growth were disclosed as new technology.[1]

APPENDIX 7

Deliveries of five samples were shipped to JPL for stress and electronic properties characterization. They were:

Ribbon 18-7 (11/24/76)	Grown on JPL No. 1. Doped to 10 Ω·cm p-type. Length submitted 15". Stress not measured. IR absorption - negligible. All system parts baked out.
Ribbon 18-8-1 (12/03/76)	Grown on JPL No. 1. Wacker crackle feed material. ~.9"/min pull speed. All system parts baked out. Solar cells to be fabricated. 2" wide easily attained.
Ribbon 14-204-1 (11/19/76)	Grown on JPL No. 2. System not pure. No dopant. Growth speed 2.0" - 2.4"/min. Buckling every 0.9". Residual stress fairly large.
Ribbon 14-205-2	Grown on JPL No. 2. System not pure. Growth rate 2.0" - 2.3"/min. Doped to 1 Ω·cm p-type. Buckling every 1.1". No residual stress.
Ribbon 18-4-4 (10/21/76)	Grown on JPL No. 1. Doped to 1.0 Ω·cm p-type. Dow Corning ingot feed material. Electronic characterization*. Resistivity: 1.1 Ω·cm. Mobility: 226 cm^2/V-sec. Carrier concentration: 2.51 x 10^{16} cm^{-3}. Growth rate 1.7"/min. Length submitted 17". Stress not measured. D_L: too small to measure. Main heating element and crucible holder not baked out. Solar cell data to follow. Crucible holder and main heater not baked out.

*Monthly Progress Report covering period October 1, 1976 - October 31, 1976.

Table X. Updated Program Plan

*Financial and Technical Reports Solar Cells and Samples will be delivered as per the Delivery Schedule of this contract.

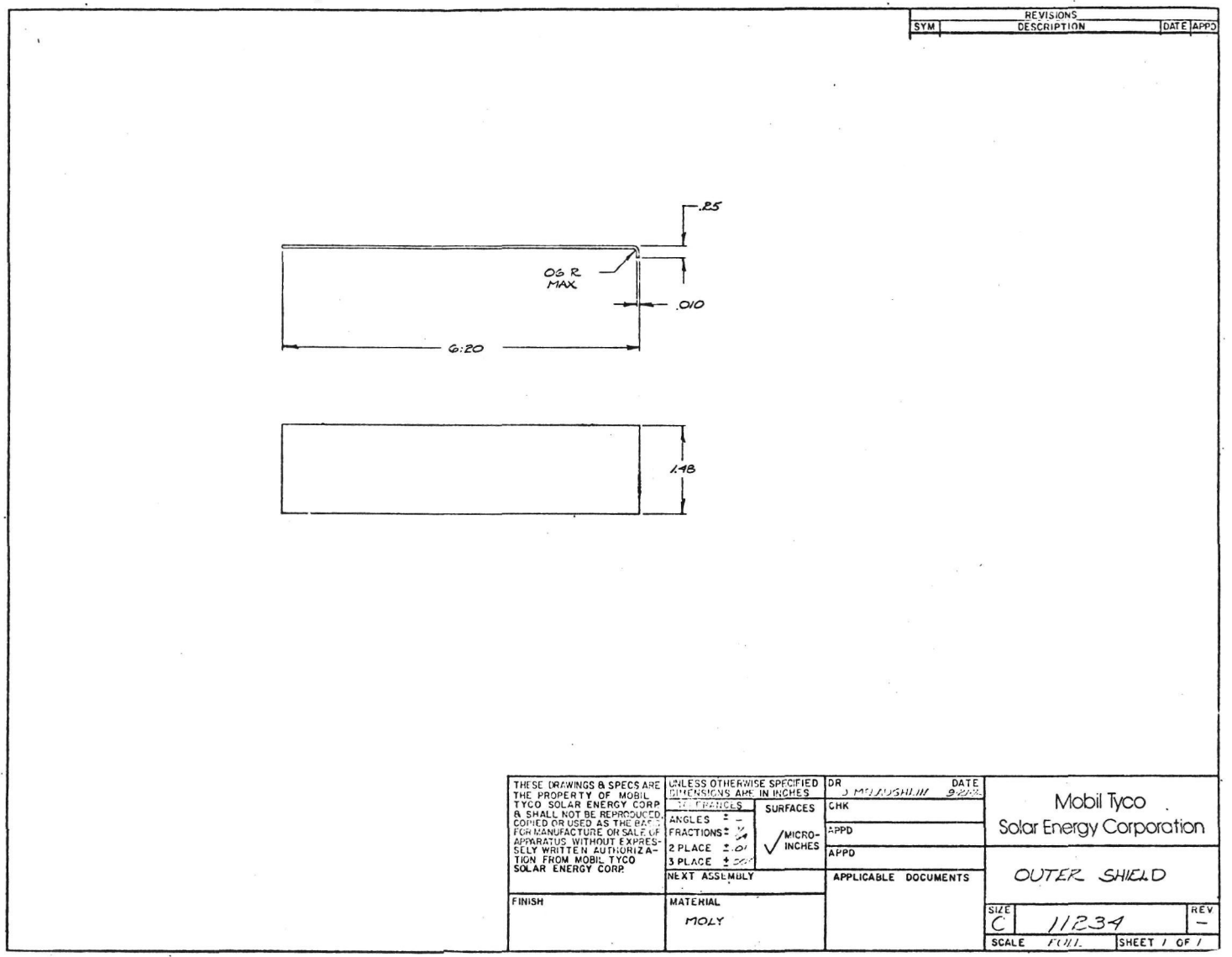

Fig. 27. Outer shield.

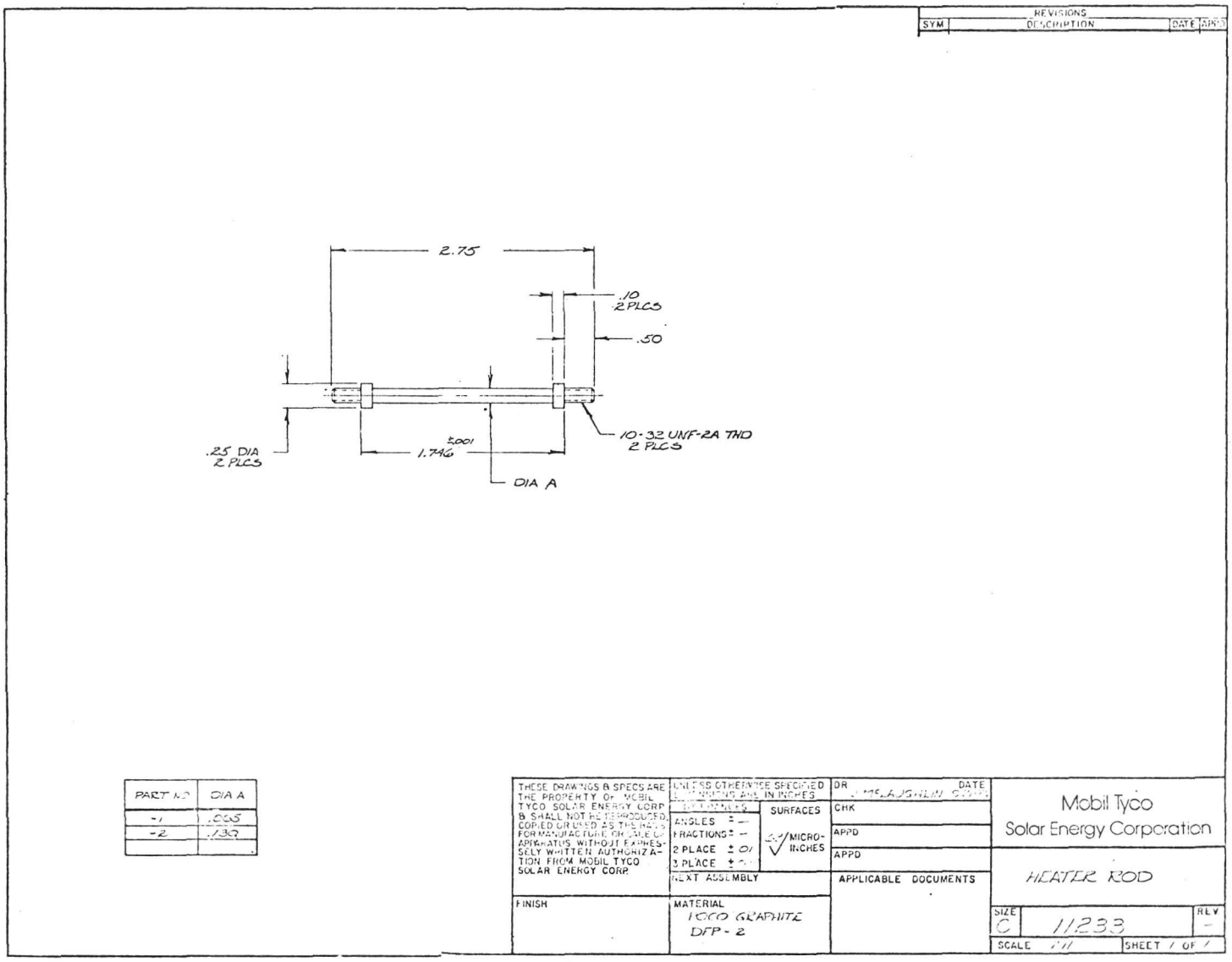

Fig. 28. Heater rod.

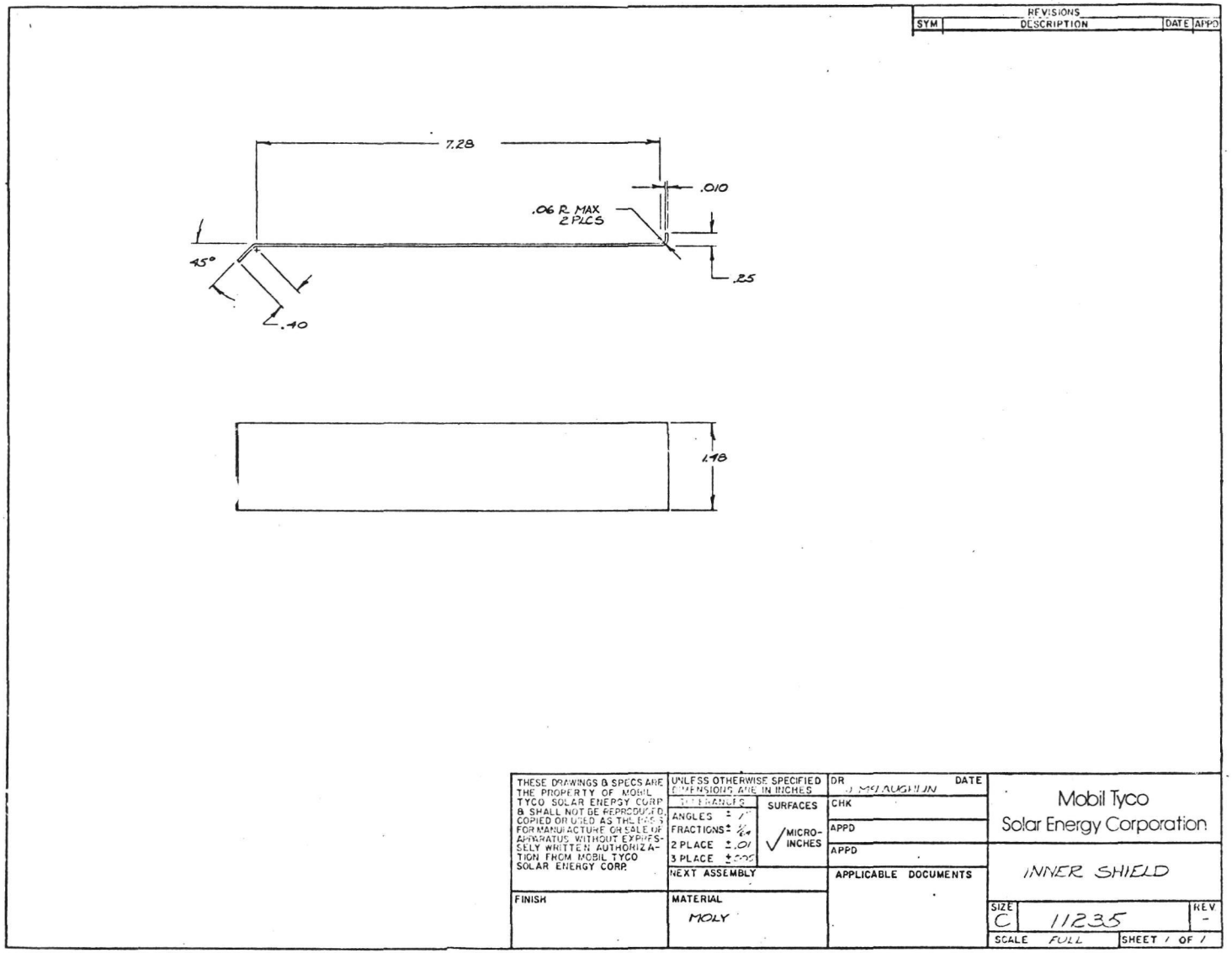

Fig. 29. Inner shield.

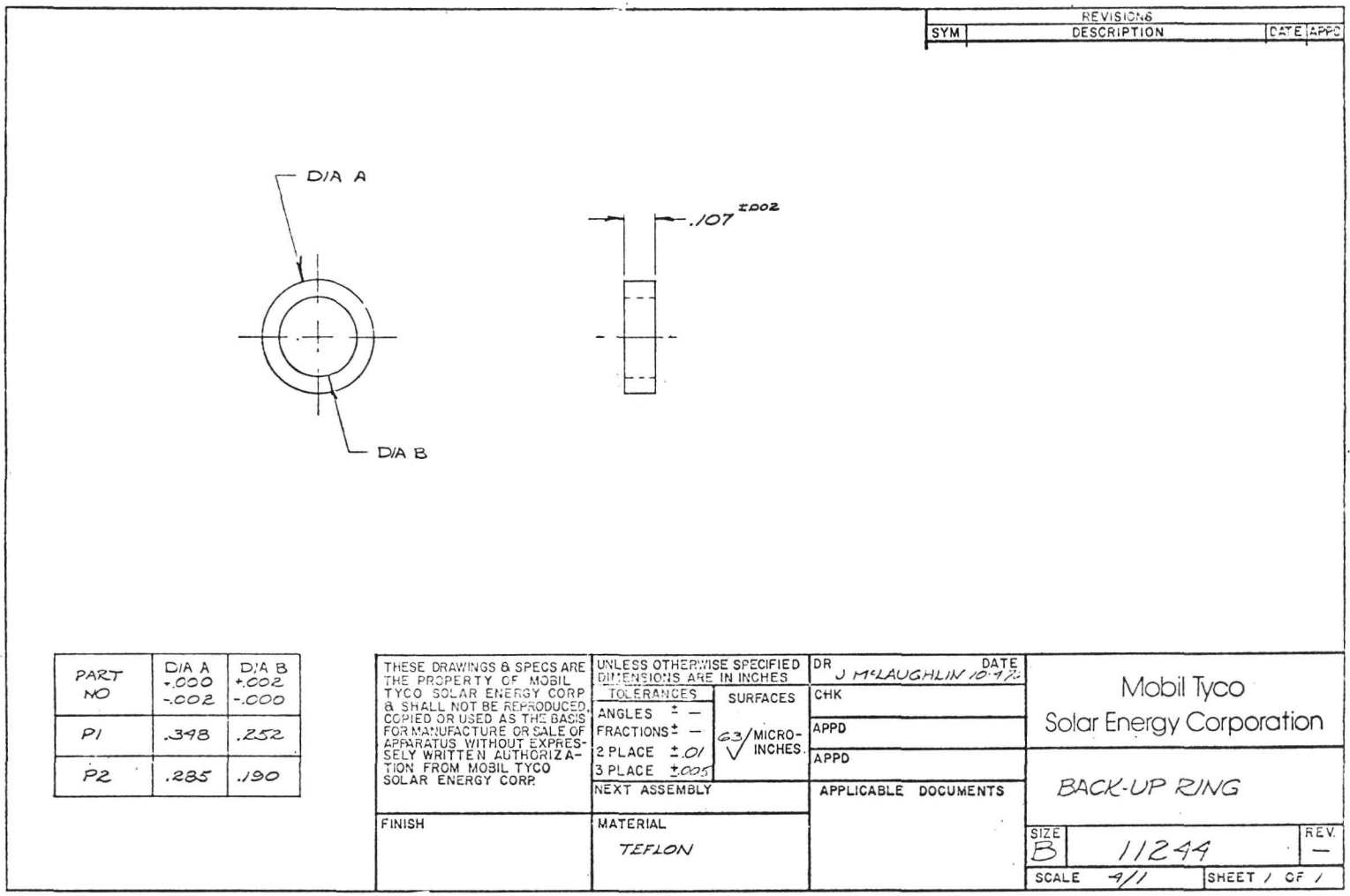

Fig. 30. Back-up ring.

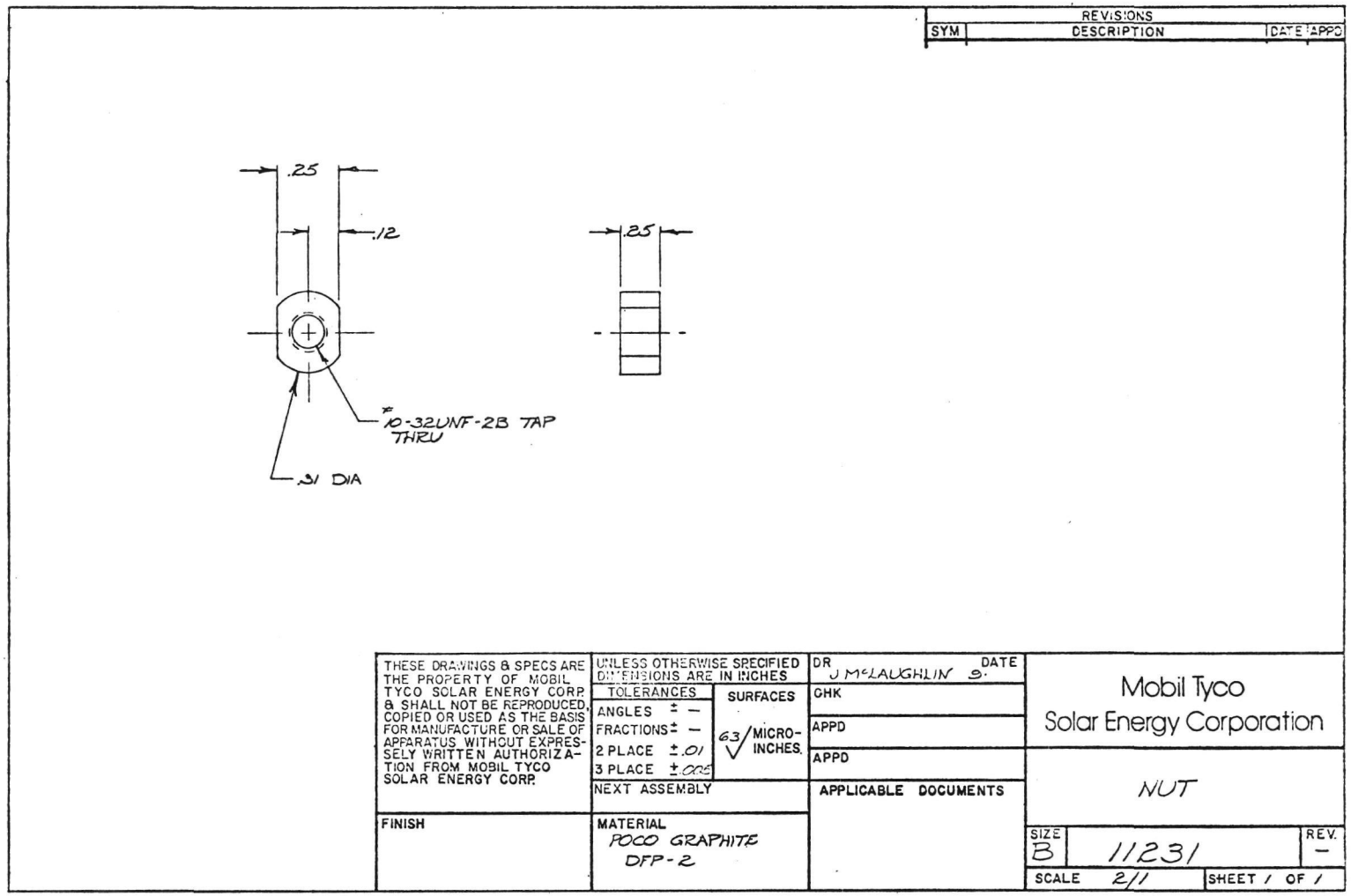
REVISIONS
SYM
DESCRIPTION
DATE
APPD
.25
.12
.25
#10-32UNF-2B TAP THRU
.51 DIA
THESE DRAWINGS & SPECS ARE THE PROPERTY OF MOBIL TYCO SOLAR ENERGY CORP. & SHALL NOT BE REPRODUCED, COPIED OR USED AS THE BASIS FOR MANUFACTURE OR SALE OF APPARATUS WITHOUT EXPRESSELY WRITTEN AUTHORIZATION FROM MOBIL TYCO SOLAR ENERGY CORP.
UNLESS OTHERWISE SPECIFIED DIMENSIONS ARE IN INCHES
TOLERANCES
ANGLES ± —
FRACTIONS ± —
2 PLACE ± .01
3 PLACE ± .005
SURFACES
63 √ MICRO-INCHES
NEXT ASSEMBLY
FINISH
MATERIAL
POCO GRAPHITE
DFP-2
DR J McLAUGHLIN 9- DATE
CHK
APPD
APPD
APPLICABLE DOCUMENTS
Mobil Tyco
Solar Energy Corporation
NUT
SIZE B
11231
REV. —
SCALE 2/1
SHEET 1 OF 1

Fig. 31. Nut.

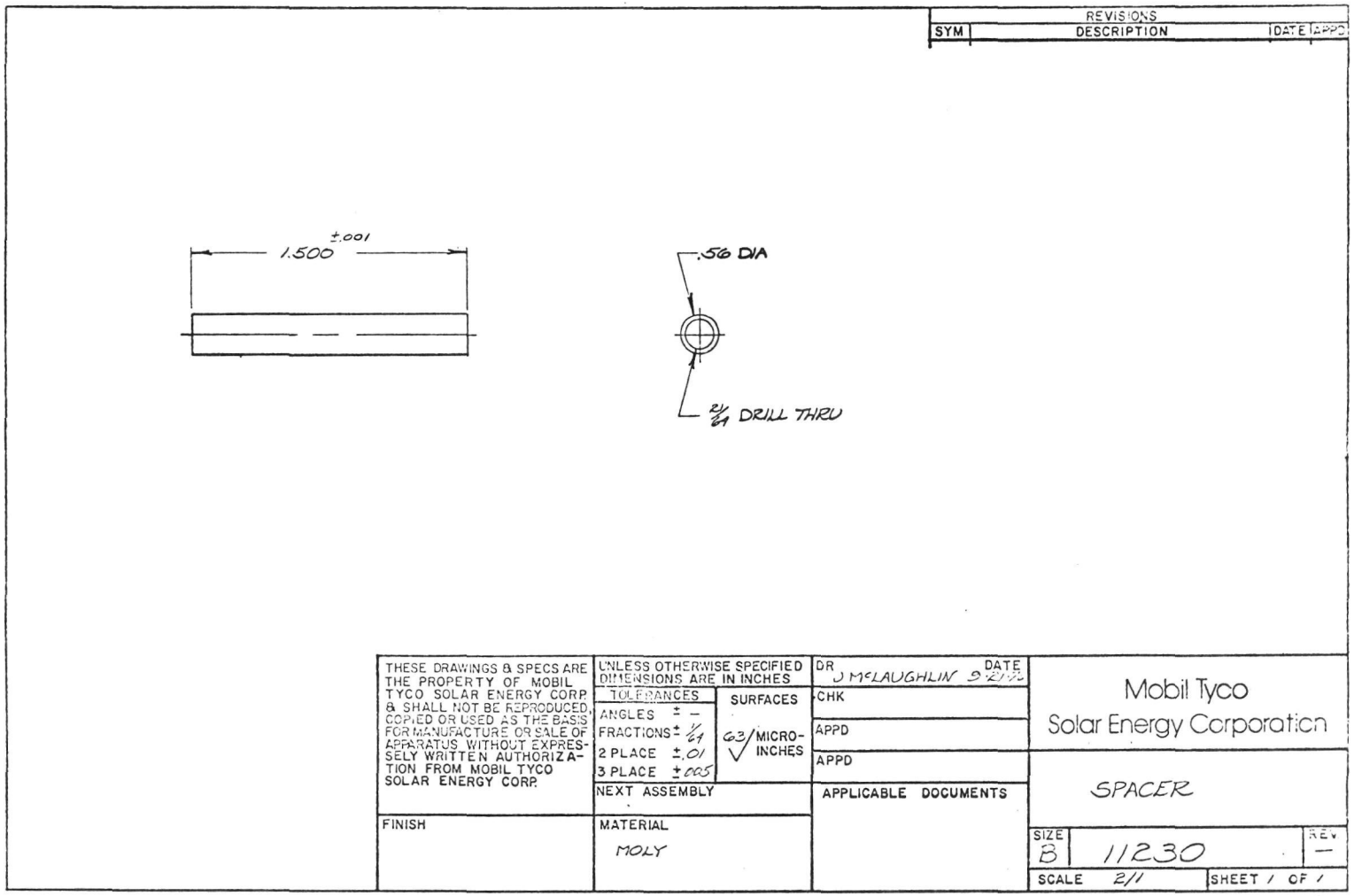

Fig. 32. Spacer.

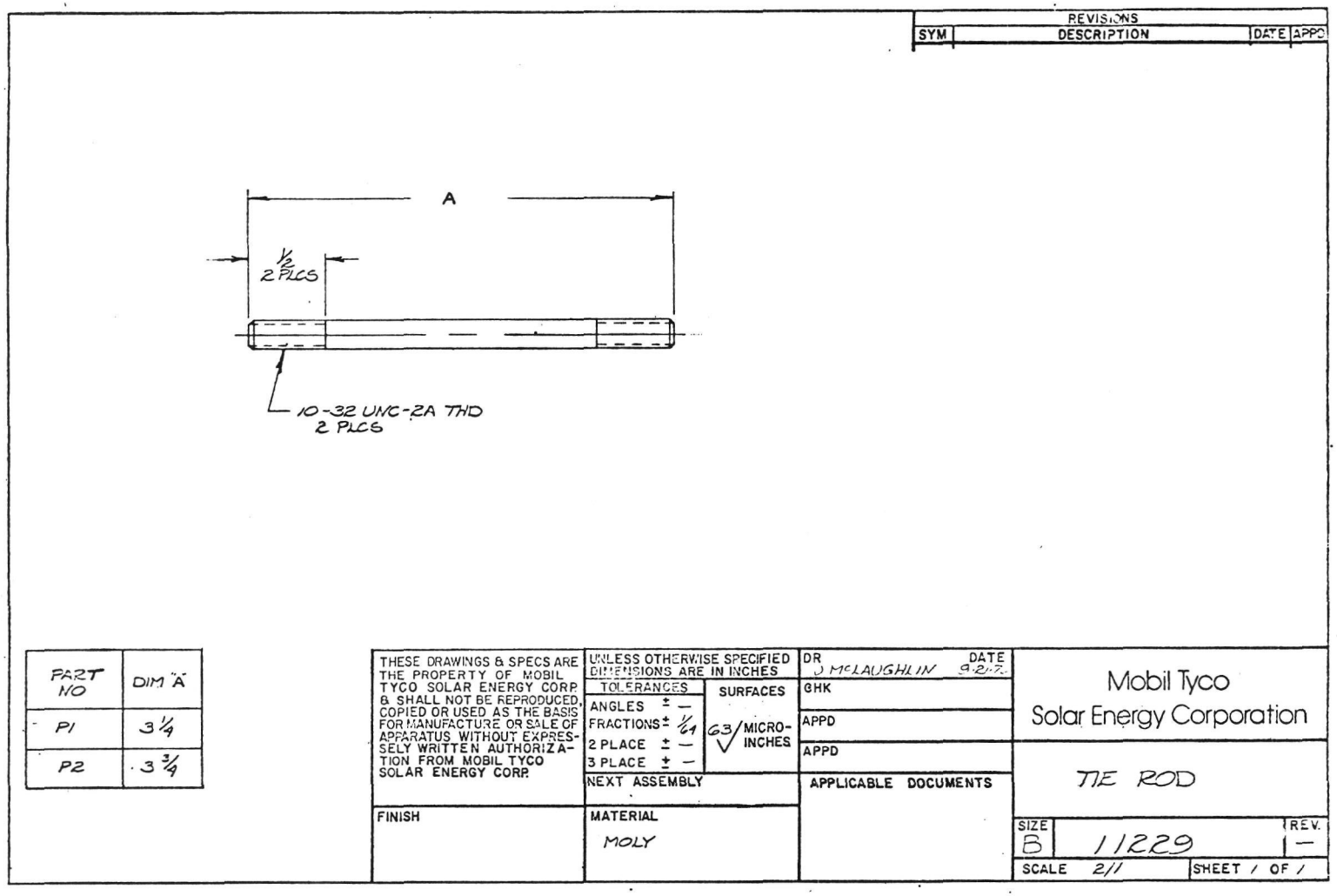

Fig. 33. Tie rod.

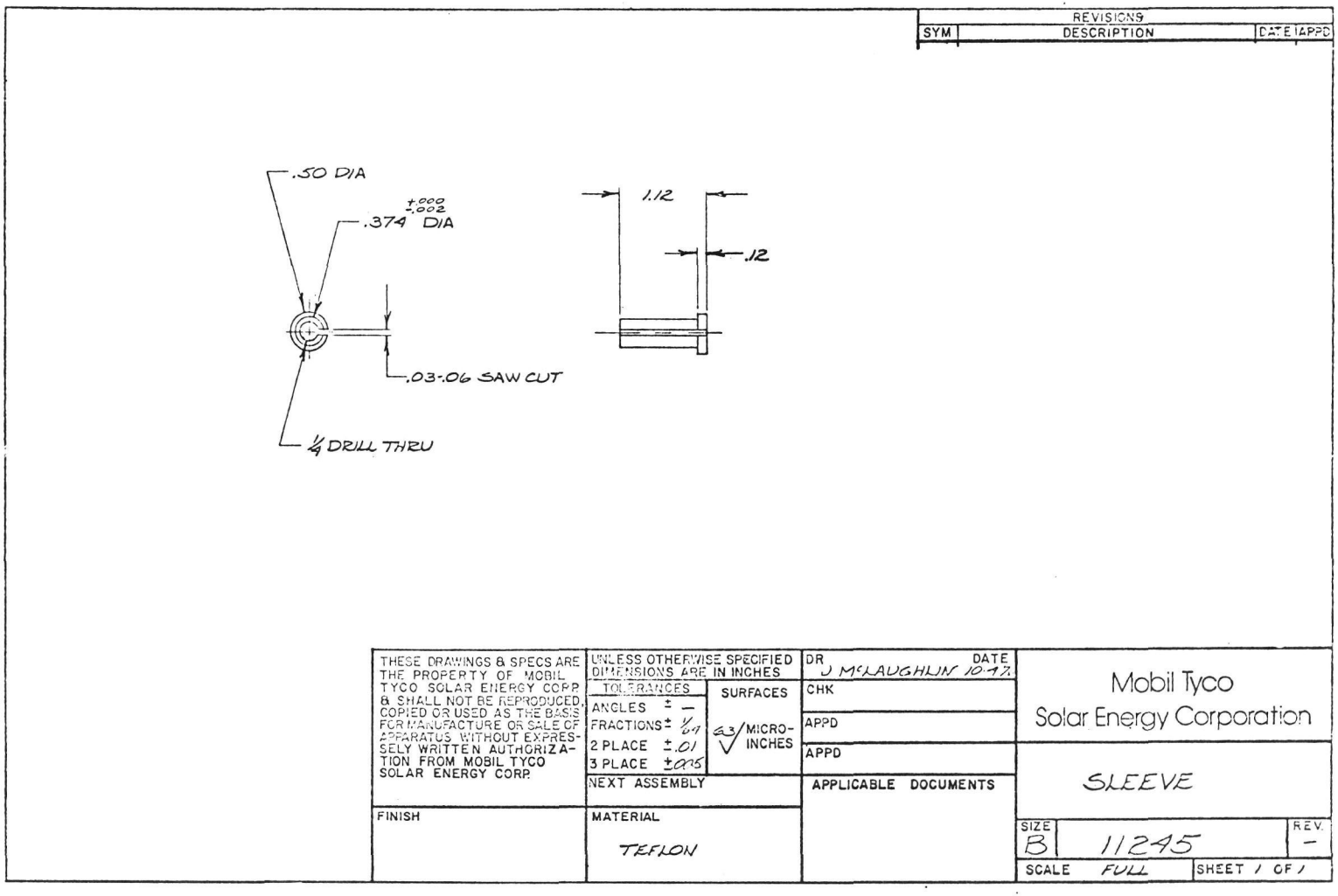

Fig. 34. Sleeve.

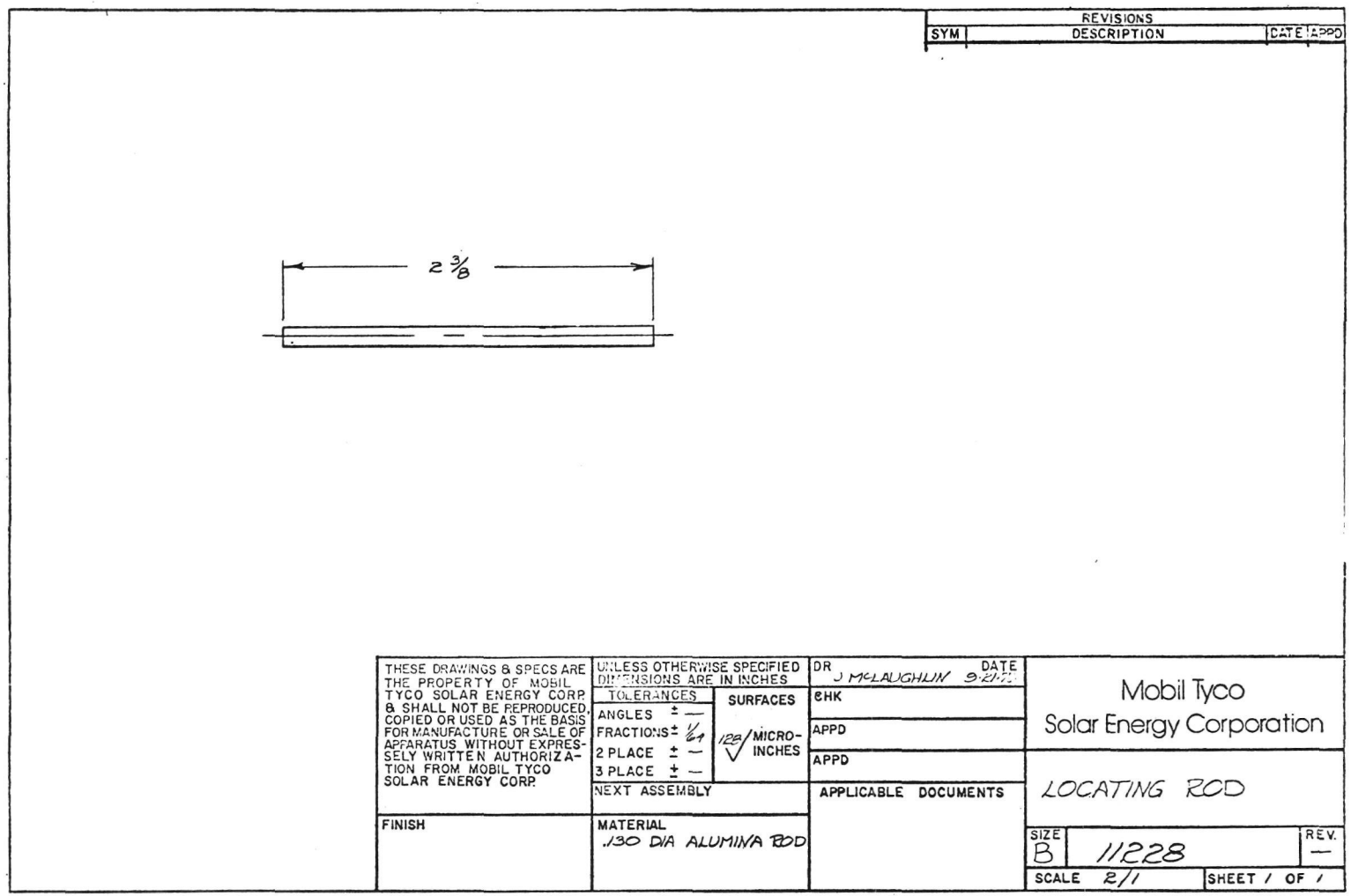

Fig. 35. Locating rod.

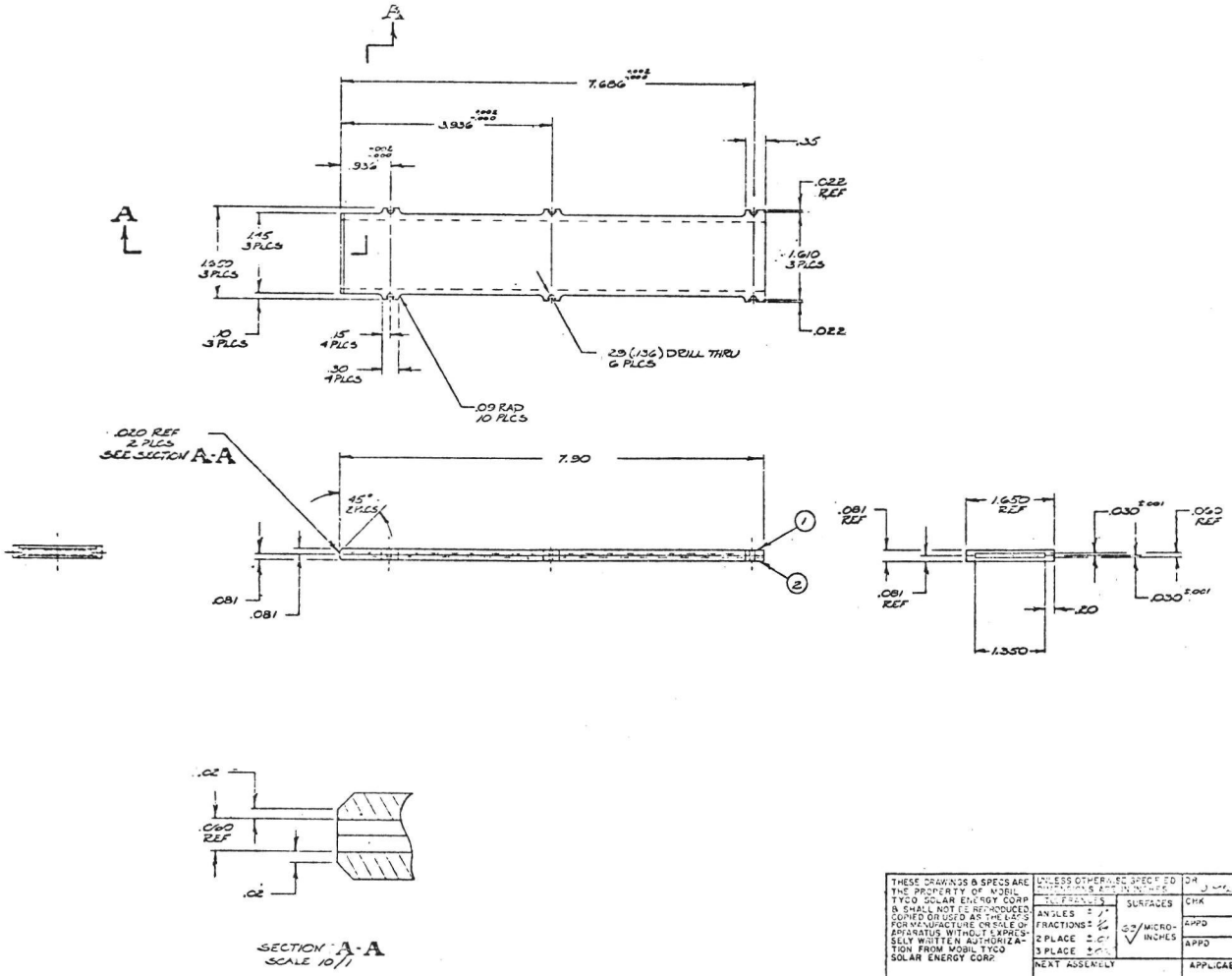

Fig. 36. Heater.

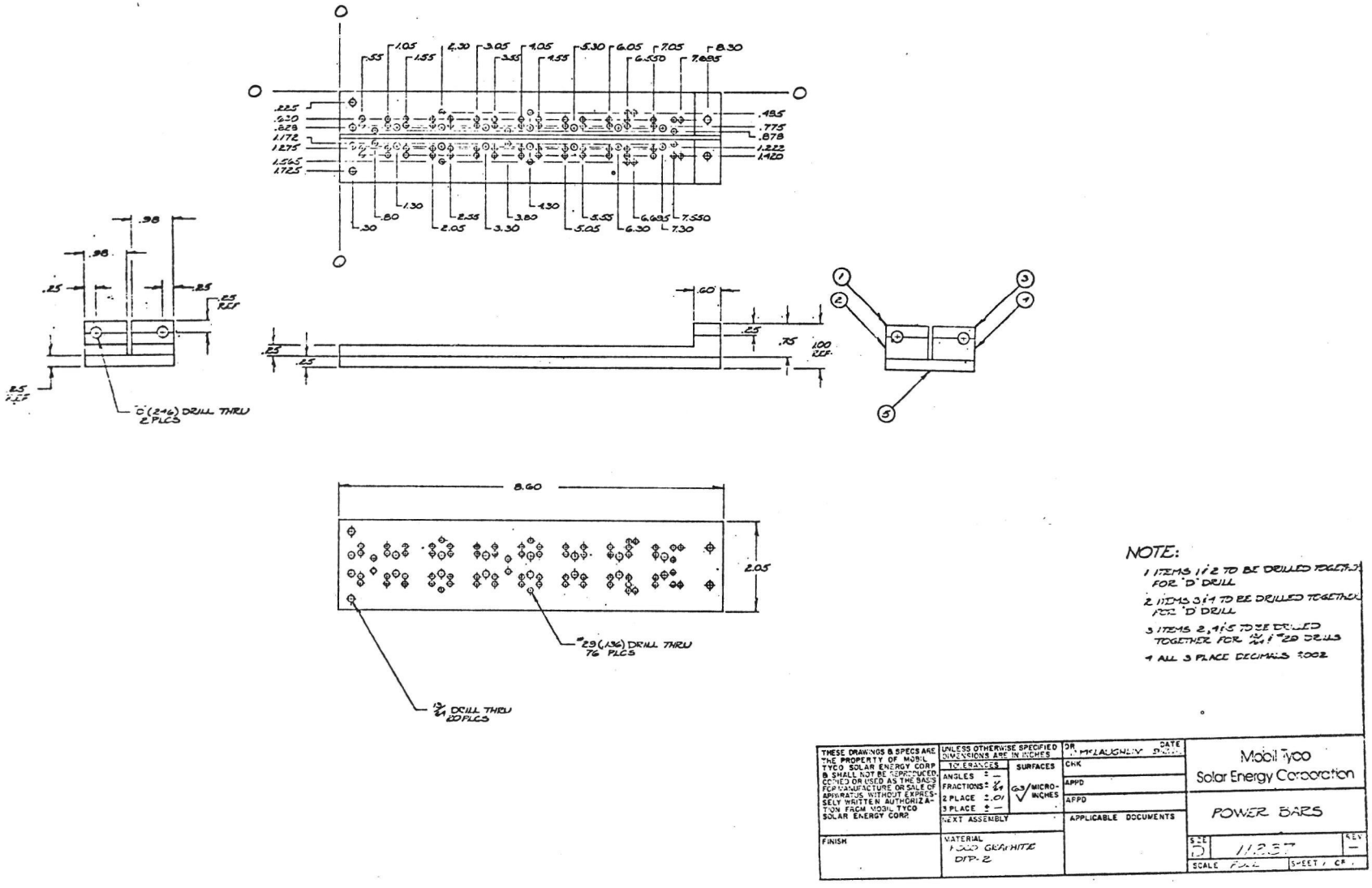

Fig. 37. Power Bars.

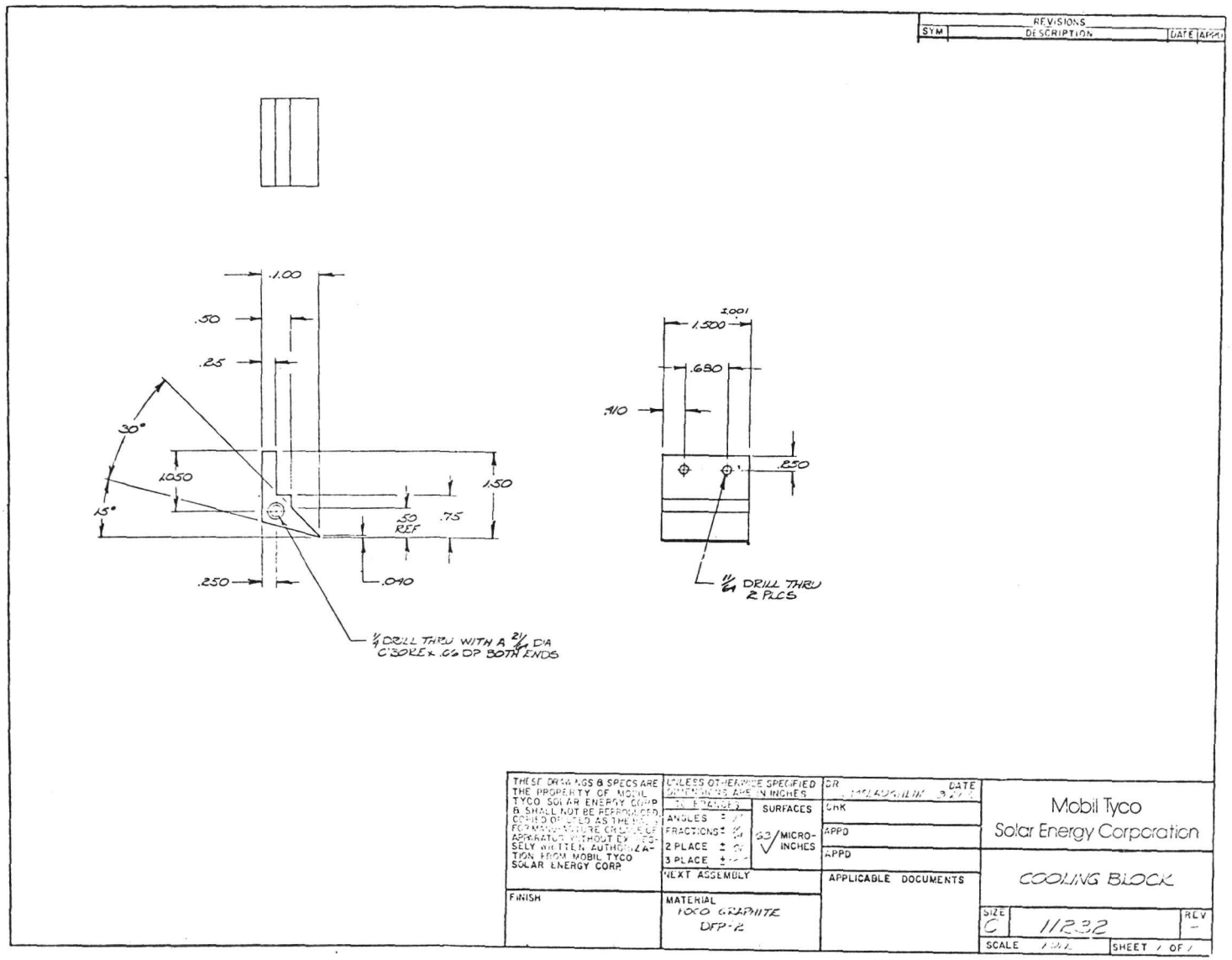

Fig. 38. Cooling block.